이학박사 학위논문

대사 및 DNA 손상 조건에서 p53 및 히스톤 수식화 조절

p53 and histone modification regulation on cellular metabolism and DNA damage

2015 년 02 월

서울대학교 대학원

의과학과 의과학전공

이 종 혁

A thesis of the Degree of Doctor of Philosophy

p53 and histone modification regulation on cellular metabolism and DNA damage

대사 및 DNA 손상 조건에서 p53 및 히스톤 수식화 조절

February 2015

The Department of Biomedical Sciences

Seoul National University

Graduate School

Jong-Hyuk Lee

대사 및 DNA 손상 조건에서 p53 및 히스톤 수식화 조절

지도 교수 윤 홍 덕

이 논문을 이학박사 학위논문으로 제출함

2014년 10월

서울대학교 대학원

의과학과 의과학전공

이 종 혁

이종혁의 이학박사 학위논문을 인준함

2014년 12월

위 원 장 _____ (인)

부위원장 _____ (인)

위 원 _____ (인)

위 원 _____ (인)

위 원 _____ (인)

p53 and histone modification regulation on cellular metabolism and DNA damage

by

Jong-Hyuk Lee

A thesis submitted to the Department of Biomedical Sciences
in partial fulfillment of the requirements for the Degree of Doctor
of Philosophy in Science at Seoul National University Graduate School

December 2014

Approved by Thesis Committee:

Professor _____

Chairman

Professor _____Vice chairman

Professor _____

Professor _____

Professor _____

ABSTRACT

Post-translational modifications of proteins alter the characteristics of protein, supporting its original function or perform another. Histone, which binds DNA and consist chromatin structure undergoes diverse post-translation modifications. These modifications mainly take place on N-terminal tails of core histones, and alter the electrostatic nature of histones regulating the physical binding of transcription factors or providing a binding spot of transcription factor complex on itself, playing central role in transcription regulation.

p53, especially, is called ‘guardian of genome’ which plays key role in suppressing cellular oncogenesis and promotes genomic stability. p53 also undergoes various post-translational modifications to regulate cell-cycle arrest, DNA-repair, apoptosis.

First, novel histone modification, which takes place under DNA-damaging conditions, was explored. We found that histone H3 threonine 45 (H3-T45) was phosphorylated by cellular signal transduction protein AKT under various DNA-damaging agents. AKT is a serine/threonine kinase which transfers hormone or growth factor signal to induce cellular proliferation and is a key molecule involved in cellular oncogenesis. AKT is also known to be phosphorylated and activated under DNA-damaging conditions and induces *CDKN1A* transcription. By genome-wide chromatin immunoprecipitation sequencing (ChIP-seq) analysis, H3-T45 phosphorylation was distributed throughout the DNA damage responsive gene locus, particularly immediately after the transcription termination site (TTS). H3-T45 phosphorylation overlapped extensively with RNA polymerase II C-terminal domain (CTD) serine 2 phosphorylation, which establishes the transcription termination signal. AKT1 was more effective than AKT2 in H3-T45 phosphorylation. Blocking H3-T45 phosphorylation by inhibiting AKT or through amino acid substitution decreased RNA decay downstream of mRNA cleavage sites and RNA polymerase II release from chromatin. Our findings suggest that AKT-mediated phosphorylation of H3-T45 correlates with the termination of transcription on DNA damage.

Second, ATP citrate lyase (ACLY), which controls cellular senescence through p53, was studied. ACLY catalyzes cytosolic citrate into acetyl-coA, involved in cellular fatty acid synthesis and ACLY inhibition caused retarded proliferation of cancer cell. Recent study revealed that ACLY affects overall

cellular gene expression profiles though regulating histone acetylation by acetyl-CoA production. In this study, we found that inhibition of ACLY in normal cells showed senescent morphology which is caused by p53. Acetyl-CoA back-up in ACLY knockdown cells was not sufficient to recover from the senescent phenotype. Moreover, ACLY directly interacted with the catalytic subunit of AMPK and suppressed its activity. As well as normal cells, knockdown of ACLY in cancer cells showed increased p53 level which resulted in induced apoptosis under DNA-damaging condition. Throughout this study, we identified a novel function of ACLY which interconnects cellular energy sensor AMPK and tumor suppressor p53 in cellular senescence and tumorigenesis.

Keywords: ATP-citrate lyase (ACLY), p53, AMP-activated protein kinase (AMPK), senescence, tumor, AKT, histone, phosphorylation, DNA-damage, transcription, transcription termination

Student number: 2009-30609

CONTENTS

LIST OF FIGURES

Chapter 2

Chapter 3

LIST OF TABLES

Chapter 2

Chapter 3

LIST OF ABBREVIATIONS

H3T45p	**Phosphorylated 45th threonine of histone H3**
DMSO	**Dimethyl sulfoxide**
ETPS	**Etoposide**
ADR	**Adriamycin**
ChIP-seq	**Chromatin immunoprecipitation-sequencing**
TSS	**Transcription start site**
TTS	**Transcription termination site**
ACLY	**ATP-citrate lyase**
ACSS	**Acetyl-CoA synthetase**
AMPK	**AMP-activated protein kinase**
HDF	**Human dermal fibroblast**
SA-β-gal	**Senescence-associated beta-gal**
scr	**Scrambled**

CHAPTER 1

General introduction

Every living organism reacts to diverse stimulations in various actions to overcome the environmental stresses, and it is the fundamental characteristic of ‘life’ that maintains homeostasis. Gene transcription is the first step and a key feature in maintaining homeostasis.

Genetic code, which lies within genomic DNA is transcribed into RNA transcript, and translated into protein product to express its information. Hence, transcription regulation has the highest priority in maintaining the homeostasis.

Total length of the human genomic DNA spans approximately 2 meters in length. Eukaryotes are evolved to form higher-order nuclear scaffolds to ‘pack’ the genomic DNA into relatively limited nuclear space which spans only 6 micrometers. DNA is wrapped around the core histone proteins like ‘beads on a string’. Histone proteins are overall positively charged by harboring basically charged amino acids, while DNAs are negatively charged. Each core histones (H2A, H2B, H3, and H4) harbor the ‘tail structure’ on their N-terminus, which are exposed to nuclear-plasm and undergoes various post-translational modifications (PTMs). N-terminal tail modifications are especially important in transcription regulation as their modifications alter the overall charge of core histone, affecting the electrostatic interaction force with the inbound genomic DNA. Also, the N-terminal tail acts as a barrier or the docking site of transcription factors. So, it is highly important to study the precise mechanism of histone modification and transcription regulation.

In this context, histone modification under DNA damaged and metabolically manipulated conditions are studied.

DNA damage stimulates diverse cellular response to recover cells from damage. If the damage is so severe and exceeds the capability to recover, cells undergo apoptosis, which is a 'self-destruct switch' toward tumorigenesis. Histone phosphorylation by DNA damage is mostly studied on the point of DNA break. Moreover, the relationship between DNA damage-induced histone phosphorylation and transcription regulation, which is the major part of histone modification, remains poorly understood.

At the beginning, we focused on 45th threonine of core histone H3 (H3-T45), which is known to be phosphorylated by PKCδ, CDC7, DYRK1A under diverse circumstances. Since amino acid sequence of H3-T45 showed typical AKT substrate motif, we questioned whether this site is actually phosphorylated by AKT.

Next, we silenced ATP-citrate lyase (ACLY), which is the key enzyme in cellular acetyl-CoA production, to discover the relationship with histone acetylation. However, we discovered unexpected consequence of ACLY knockdown, which is predicted to be the cellular senescence. And the nature of molecular mechanism underlying ACLY silencing-driven cellular senescence is studied.

CHAPTER 2

DNA damage-activated AKT Phosphorylates H3-threonine 45 to facilitate gene transcription termination

1. INTRODUCTION

Mammalian core histone undergoes various post-translational modifications (PTMs). These modifications mainly occur on N-terminal tails of histone because of the structural feature which is open-access to modifying enzymes (1,2). Most abundant modifications include acetylation, methylation, phosphorylation, ubiquitination etc (3). These PTMs are crucial step, especially in epigenetic regulation of a gene, through controlling the association of transcriptional factors to inbound DNA.

Phosphorylation, especially, is emerged as indispensable modification recently. Conventionally, H3-S10 phosphorylation is known as a critical factor during mitogenesis (4). Phosphorylation of H3-Y41 by JAK2 excludes HP1α from chromatin, activating transcription from repressed state (5). PKC-β1 controls demethylation at H3-K4 by H3-T6 phosphorylation, maintaining transcription activation (6). H3-T11 phosphorylation is also extensively studied. DNA damage responding kinase Chk1 phosphorylates H3-T11, maintaining transcription activation under normal conditions (7). However, DNA damage signal releases Chk1 from chromatin and blocks transcription of cell cycle related genes such as cdk1, Cyclin B1, etc. Metabolic enzyme PKM2 also phosphorylates H3-T11, which translocate into the nucleus by growth factor stimulation and activates transcription of genes related to cellular proliferation (8). Little is known about H3-T45 phosphorylation. There exists a study claiming PKC-δ as a histone H3-T45 kinase, which is induces upon cellular apoptosis (9). The other group reported H3-T45

phosphorylation is a replication specific marker in S. cerevisiae which is phosphorylated by yeast Cdc7, Dbf4 complex (10).

AKT, also known as Protein Kinase B (PKB) is a serine / threonine kinase which plays central role in cellular oncogenesis. AKT is fully activated by phosphorylation at T308 and S473 by PDK (phosphoinositide dependent protein kinase) 1 and 2, respectively (11). Most of the effects of phosphorylation on AKT regulation have been studied only in the context of hormone/growth factor signaling or development. However, AKT-S473 is also phosphorylated in response to various genotoxic stresses by PI3K like kinase (ATM, ATR) or DNA-PK (12-15). DNA-dependent protein kinase (DNA-PK) is known to phosphorylate AKT under IR or UV irradiation, inducing expression of p21 (CDKN1A) to promote cell survival (16). Once activated, AKT regulates cellular survival and metabolism by binding and regulating many downstream effectors, e.g. NF-kappa B, Bcl-2 family proteins, MDM2, GSK3, FoxO1 and CDKN1A (17-22).

mRNA transcription via RNA polymerase II (PolII) processes through series of tightly regulated reactions, which is controlled via its C-terminal domain (CTD) phosphorylation (23). CTD contains heptad peptide sequence YSPTSPS, which repeats 26 and 52 times in yeast and in human, respectively (24). The CTD at the promoter of actively transcribed genes are unphosphorylated. PolII-S5 phosphorylation occurs to recruit 5' capping enzymes at the stage of early initiation, PolII-S2 phosphorylation increases

while PolII-S5 phosphorylation decreases, during transcription elongation and PolII-S2 phosphorylation predominates to recruit transcription termination factors, which are required for mRNA cleavage and polyadenylation.

Transcription termination process is prerequisite for genome partition and precise expression of neighboring genes (25). Particularly, 3' end processing is an essential step in mRNA maturation, splicing and transcription termination (26). Two models were proposed to provide the explanation between 3' end processing and RNA PolII transcription termination. The first one is called 'allosteric' or 'anti-terminator' model (27). This model proposes that, when RNA PolII transcription progresses through the poly(A) site, elongation complex undergoes the conformational change which leads to dissociation of elongation factors and association of termination factors. Second one is referred to as 'torpedo' model (28). In this model, mRNA cleavage at poly(A) site generates unprotected downstream RNA product, which is attacked by 5'-3' exonucleases. And the exonuclease (torpedo) catches up the RNA PolII to release from the chromatin. However, emerging evidences claim that the transcription termination mechanism more likely reflects a complex combinatorial action of both models (29). Regardless of its importance, termination is the least understood step in transcription process. Further, the relationship between transcription termination and histone modifications is unknown.

Although AKT is generally known as cytosolic protein, there are some key evidences demonstrating AKT plays important role within the nucleus. Also, there are no previous data claiming interaction of AKT and nucleosome core histones. Furthermore, none of the studies connect histone modification with transcription termination.

In this study, we demonstrate that AKT phosphorylates the 45-threonine residue of histone H3 upon DNA damage and AKT-mediated phosphorylation of H3-T45 regulates transcription termination. These findings provide an unexpected function of AKT, as a histone kinase, in transcription termination of genes upon DNA damage.

2. MATERIALS AND METHODS

1. Cell culture and transient expression

HEK293T, HeLa, MCF7, and MCF10A cells were obtained from ATCC. Except for the MCF10A cells, cells were cultured in Dulbecco's modified Eagle's medium supplemented with 10% (v/v) fetal bovine serum and antibiotics. MCF10A cells were cultured in DMEM-F12 media supplemented with 5% (v/v) fetal bovine serum, L-glutamine, antibiotics, insulin (20μg/ml, Sigma), Cholera toxin (0.1μg/ml, Listbiological Labs), Hydrocortisone (1μg/ml, Sigma), hEGF (0.02μg/ml, PeproTech). Polyethylenimine (PEI, Polysciences) was used to transfect HEK293 and HeLa cells. MCF10A cells were electrophoresed with the Neon Transfection System (Invitrogen), according to the manufacturer's instructions.

2. DNA constructs and purification of recombinant proteins

Mammalian expression vectors for dominant negative (DN) and Myristoylated (Myr) AKT1 are purchased from Millipore. Expression vectors for H3 WT, T45A were generated by subcloning PCR fragment into Platinum-A (Plat-A) cell line and MCF10A cells stably overexpressing these clones were generated as manufacturer's instructions (CELL BIOLAB, INC.). Proteins of core histones were generated by subcloning PCR fragment into pGEX4T-1 (Amersham Biosciences) or pRSETB (Invitrogen). GST fusion proteins were expressed in the *Escherichia-coli* strain *DH5α* and proteins were isolated using Glutathione Sepharose™ 4B beads (Amersham Biosciences), according to the manufacturer's instructions. His_6 fusion

proteins were expressed in the strain *BL21DE*3 and proteins were purified with Ni-NTA agarose (Quiagen), according to the manufacturer's instructions.

3. Antibodies and reagents

Anti-Actin antibodies were purchased from Sigma; anti-Myc (9E10) from Covance; anti-H3, anti-H3 (phosphorylated-T45, trimethylated-K36) from Abcam; anti-H2A, anti-H2B, anti-H3 (phosphorylated-S10), anti-H2A/H4 (phosphorylated-S1), anti-H2AX (phosphorylated-S139) from upstate; anti-H2B (phosphorylated-S36) from ECM Biosciences; anti-phosphorylated RNA PolII-S2 (3E10) and anti-phosphorylated RNA PolII-S5 (3E8) from Millipore; anti-p53 (DO-1, FL393) and anti-Rpb1 from Santa Cruz; anti-AKT1, anti-AKT2, anti-pan AKT and anti-AKT (phosphorylated-S473) from Cell Signaling. Rabbit polyclonal H3-T45 phosphorylation-specific antibody was generated from Openbiosystems (Thermofisher scientific) by immunizing phosphorylated H3-T45 peptide into 3 SPF rabbits. Anti-H3s (phosphorylated-T3, T11, S28) were a generous gift from Dr. Kyong-Tai Kim (Department of Life Science, Division of Molecular & Life Science, Pohang University of Science and Technology).

4. Lentiviral sh-RNA-mediated knockdown

Lentiviral vectors containing the human AKT1-targeting sequences pLKO.1-sh-AKT1 #1 (TRCN0000010171), #2 (TRCN0000010174), #3 (TRCN0000039794), #4 (TRCN0000039795), and #5 (TRCN0000039793) and AKT2 pLKO.1-sh-AKT2 #1 (TRCN0000000563), #2

(TRCN0000039968), #3 (TRCN0000265834), #4 (TRCN0000265848), and #5 (TRCN0000265851), CDC7 pLKO.1-sh-CDC1 #1 (TRCN0000196970), #2 (TRCN0000003171), #3 (TRCN0000196543), and #4 (TRCN0000350364) and PKC-δ pLKO.1-sh-PKC-δ #1 (TRCN0000284800), #2 (TRCN0000379731), #3 (TRCN0000101202), and #4 (TRCN000010193), and DYRK1A pLKO.1-sh-DYRK1A #1 (TRCN0000010611), #2 (TRCN0000010612), #3 (TRCN0000010613), and #4 (TRCN0000010614) were purchased from Sigma. As a control, the pLKO.1 vector was used. Lentivirus was produced according to the manufacturer's protocol using the BLOCK-iT Lentiviral RNAi expression system (Invitrogen). Twenty-four hours after lentiviral infection, infected cells were selected with puromycin (1 μg/ml) for 2 weeks and then used for experiments. Because pLKO.1-sh-AKT1 #3, pLKO.1-sh-AKT2 #2 pLKO.1-sh-CDC7 #2, pLKO.1-sh-PKC-δ #4, and pLKO.1-sh-DYRK1A #1were most effective, we used it in most experiments, where it is not specifically noted.

5. AKT1 kinase assay

Anti-Myc conjugated protein G agarose bead was used to immunoprecipitate HEK293T cells overexpressing DN/Myr-AKT in total cell lysates. Immunoprecipitated protein G agarose bead or active AKT1 (upstate) was mixed with substrate in 20mM MOPS (pH 7.2), 25mM β-glycerol phosphate, 5mM EGTA, 1mM sodium orthovanadate, 1mM dithiothreitol, 75mM $MgCl_2$, 75μM ATP, 10μCi ^{32}P-ATP (IZOTOP). Reaction mixture was incubated 2

hours at 30°C and loaded onto SDS-PAGE. Gels were dried 1 hour at 80°C and exposed on film for overnight at -80°C.

6. Immunoprecipitation and Immunofluorescent staining

Immunofluorescent staining was performed as previously described (30). For co-immunoprecipitation assays, transfected HEK293T cells were harvested 36 h post-transfection, washed in phosphate-buffered saline, and lysed in lysis buffer (20mM Tris-HCl, pH 7.4, 150mM NaCl, 1mM EDTA, 0.5% Nonidet P-40, and protease inhibitors). Cell lysates were immunoprecipitated with suitable antibodies along with Protein-A/G beads (Santa Cruz). The Immunoprecipitates were washed in lysis buffer, denatured in sodium dodecyl sulfate (SDS) loading buffer, and analyzed by Western Blot. For detecting endogenous interaction between RPRD1A and AKT/H3, DMSO, Adriamycin, Adriamycin and AKT inhibitor iv treated MCF10A cells were harvested 18 hours post-drug treatment, cross-linked with formaldehyde, quenched by addition of glycine, washed in PBS, lysed in lysis buffer (0.1% SDS, 1% TritonX-100, 1mM EDTA, 20mM Tris-Cl, pH 8.1, 150mM NaCl). Lysates were solicited with Bioruptor (Cosmo Bio Co.) and immunoprecipitated with anti-RPRD1A antibody. Presences of AKT and H3 in the immunoprecipitates were analyzed by Western Blot with corresponding antibodies. For immunofluorescent staining, cells on the cover glasses were fixed with 4% (w/v) paraformaldehyde, permeabilized with 0.5% (v/v) Triton X-100, and blocked with 2% (w/v) bovine serum albumin in phosphate-buffered saline. Endogenous or overexpressed proteins were immunostained with

corresponding antibody and Rhodamine Red-X and FITC-conjugated secondary anti-mouse or rabbit IgG antibody (Jackson Immunoresearch). 50% (v/v) glycerol containing 4′,6-diamidino-2-phenylindole solutions are loaded on the slide glass and covered with cover glass. Immunofluorescence was observed under a Zeiss LSM 510 laser scanning microscope.

7. Chromatin immunoprecipitation assay

MCF10A cells (4×10^7) were harvested, cross-linked with formaldehyde to a final concentration of 1%. Cross-linking reaction was stopped by adding glycine to a final concentration of 0.125M. Cells were harvested and washed twice with cold PBS and cytosolic fractions were eliminated with buffer A [5mM PIPES (pH 8.0), 85mM KCl, 0.5% NP-40, protease inhibitors]. Nuclear pellets were washed and resuspended in 1X Micrococcal nuclease reaction buffer [10mM Tris-Cl (pH 7.9), 5mM $CaCl_2$, 0.5mM DTT] and chromatin was digested with Micrococcal nuclease (New England Biolabs). Digestion reaction was stopped by addition of EDTA into the reaction buffer. Digested nuclear pellets were resuspended in buffer B [100mM Tris-Cl (pH 8.1), 1% SDS, 10mM EDTA, protease inhibitors] and sonicated for disruption of nuclear membrane. Prepared chromatin fraction was diluted 1/10 in IP buffer (0.01% SDS, 1.1% TritonX-100, 1.2mM EDTA, 16.7mM Tris-Cl [pH 8.1), 167mM NaCl, and protease inhibitors] and incubated overnight at 4°C. Samples were incubated with salmon sperm DNA pre-coated protein A or G bead for 2~4 hours at 4°C, washed with TSE150 [0.1% SDS, 1% TritonX-100, 2mM EDTA, 20mM Tris-Cl (pH 8.1), 150mM NaCl], TSE500 [0.1% SDS,

1% TritonX-100, 2mM EDTA, 20mM Tris-Cl (pH 8.1), 500mM NaCl], BufferIII [0.25M LiCl, 1%NP40, 1% Sodium deoxycholate, 1mM EDTA, 10mM Tris-Cl (pH 8.1)], TE(pH 8.0) for two times. Washed beads were eluted with elution buffer (1% SDS, 0.1M $NaHCO_3$), incubated overnight at 65°C with NaCl for reversal of crosslinking. Samples were incubated 50°C in addition of 10μl of 0.5M EDTA, 20μl of 1M Tris (pH 6.5), and 4μl of Proteinase K (20mg/ml), purified with phenol/chloroform/isoamyl alcohol. Nucleic acid was precipitated by centrifugation 30 min at 4°C with 1μl glycogen solution (20mg/ml), 20μl NaCl (5M), and 500ul isopropanol. Pellets were washed with 70% EtOH, dried and eluted with pure water.

8. ChIP sequencing

MCF10A cells were ChIPed with anti-phosphorylated H3-T45, anti-phosphorylated RNA PolII-S2, S5, anti-H3-K36me3. Sequencing and analysis of ChIPed DNAs were performed by BML (Bio Medical Laboratories, Korea) and KRIBB (Korean Research Institute of Bioscience & Biotechnology). Briefly, DNA fragments were ligated to a pair of adaptors for sequencing on the Illumina Hiseq-2000. The ligation products were size fractioned to obtain 200–300 bp fragments on a 2 % agarose gel and subjected to 18 cycles of PCR amplification. Each library was diluted to 8 pM for 76 cycles of single-read sequencing on the Illumina Hiseq-2000 following the manufacturer's recommended protocol.

9. ChIP-sequencing data analysis

Reads after sequencing were mapped against to the human genome (GRCh37/hg19) using Bowtie v.2.1.0 (31) with the default parameters. The SAM format outputs were sorted by genomic coordinates and uniquely mapped reliable reads were used in subsequent processes. Preprocessing of SAM files was performed by Picard (http://picard.sourceforge.net). We used MACS v.1.4.2 tool (32) to select enriched region for RNA PolII and histone modification regions. We applied default settings and found significant regions (P-value <= 10-5) compared to matched control samples. Using HOMER (33), H3-T45 phosphorylation peaks were annotated for promoters, exons, introns, intergenic regions and other features according to RefSeq transcripts. GO annotation was performed using GREATv2.0.2 (34). Average normalized tag count distribution around coding gene locations were plotted using ngs.plot (35).

10. Quantitative Real-time PCR (qPCR) / conventional PCR analysis of relative mRNA levels and ChIP products

Total RNA was extracted with TriZol® (Invitrogen) and reverse-transcribed (for mRNA real-time qPCR analysis; AMV Reverse Transcriptase XL, Life science, Co., for conventional PCR analysis; Superscript III, Invitrogen). mRNA levels and antibody bound chromatin levels by chromatin immunoprecipitation assay were quantified by real-time qPCR with the SYBR® Green qPCR Kit (Finnzymes, F-410L) on the iQ5 and CFX connect Real-time PCR Detection System (Bio-Rad) and then normalized to actin and or 1% input chromatin using the $2^{-\Delta\Delta}\mathbf{C}_T$ 2-ΔΔCT calculation method.

Conventional PCR was performed using EX Taq polymerase (Takara) with MyCycler (Bio-Rad). Sequences of the primers used for mRNA quantification were described in Table 2-1.

11. Statistics

Data are presented as means ± standard deviations and *P*-value was calculated using Student's t-test calculator (http://www.physics.csbsju.edu/stats/t-test.html). A value of $p < 0.05$ was considered statistically significant. All data presented are a representative of at least three independent experiments.

12. Nascent RNA quantification

Nascent RNA quantification was performed by Nascent RNA capture kit (Life technologies) following the manufacturer's recommended protocol. Briefly, 0.1mM 5-Ethynyluridine (EU) was treated into cell culture medium for 18 hours and total RNA was extracted with TriZol® (Invitrogen). 5μg of total RNA was biotinylated with reaction cocktail (50% v/v 2X EU buffer, 2 mM CuSO4, 0.5mM biotin azide, 10 mM reaction additive 1, 12mM reaction buffer additive 2) on vortex mixer for 30 minutes at room temperature. RNA was precipitated with glycogen, ammonium acetate, and 100% ethanol at -80℃, overnight. 1μg of biotinylated RNA was purified with streptavidine magnetic bead, washed and reverse-transcribed using Superscript III reverse transcriptase (Invitrogen), according to the manufacturer's protocol. cDNA

was treated with RNaseA (Invitrogen) at 37℃ for 30 minutes and used as a template for real-time qPCR analysis.

ACTB(Actin)	Forward	5′-GGCATCCACGAAACTACCTT-3′
	Reverse	5′-CTGTGTGGACTTGGGAGAGG-3′
CDKN1A(p21)	Forward	5′-GCAGACCAGCATGACAGATTT-3′
	Reverse	5′-GGATTAGGGCTTCCTCTTGGA-3′
AKT1	Forward	5′-ATCATGCAGCATCGCTTCTTTGCC-3′
	Reverse	5′-ATCTTGGTCAGGTGGTGTGATGGT-3′
AKT2	Forward	5′-TCATCAAAGAAGGCTGGCTCCACA-3′
	Reverse	5′-TCTCGGTCTTCATCAGCTGGCATT-3′
MDM2	Forward	5′-ATGGTGCTGTAACCACCTCACAGA-3′
	Reverse	5′-CTTGGCACGCCAAACAAATCTCCT-3′
SMAD3	Forward	5′-AGGAGAAATGGTGCGAGAAG-3′
	Reverse	5′-CAGTAGATGACATGAGGGAGC-3′
KLF5	Forward	5′-CACAAAACATCCAACCTGTCAG-3′
	Reverse	5′-CTTGTATGGCTTTTCACCAGTG-3′
CDC7	Forward	5′-AGGGATCTGTAGGCCTTTCT-3′
	Reverse	5′-GTCTTTGACTGCTTCATGAGTTTC-3′
PKC-δ	Forward	5′-ACAGCGACAAGAACCTCATC-3′
	Reverse	5′-GATCTGTCCAGGAACCTCAATC-3′

DYRK1A	Forward	5′-CTCGACATCTTCCTCCTCTACT-3′
	Reverse	5′-AACGTCCATAGCTCCATTCTG-3′
CDKN1A #1 (ChIP)	Forward	5′-TGAGGCAGAATTGCTTGAACCTGG-3′
	Reverse	5′-TTCACACAGGCTCCCAAGAAGTGA-3′
CDKN1A #2 (ChIP)	Forward	5′-CTCCCACCCCTACCTGGGCT-3′
	Reverse	5′-CAGAACCCAGGCTTGGAGCA-3′
CDKN1A #3 (ChIP)	Forward	5′-CAGTTCCTTGTGGAGCCGGA-3′
	Reverse	5′-TGTGAACGCAGCACACACCC-3′
CDKN1A #4 (ChIP)	Forward	5′-TGGGGATGTCCGTCAGAACCC-3′
	Reverse	5′-CTCCCAGGCGAAGTCACC-3′
CDKN1A #5 (ChIP)	Forward	5′-TGTCCTTTCCCTTCAGTACCCTCT-3′
	Reverse	5′-TAGGGTGCCCTTCTTCTTGTGTGT-3′
CDKN1A #6 (ChIP) Primer 3 (Fig. S10)	Forward	5′-CCTCTGCAAAGATCACCAAT-3′
	Reverse	5′-CCAGTTGCTCCATAACCTTGCC-3′
CDKN1A #7 (ChIP)	Forward	5′-TGCACAGGGCAGAGCTTTCTACTA-3′
	Reverse	5′-AAACAGGTGCAGGCTATGGGACAA-3′
CDKN1A #8 (ChIP)	Forward	5′-TGGTTAACATTCAGGCCTTGCTGC-3′
	Reverse	5′-ATGGCCACTGTCGATGGAGACATT-3′
RT primer (Fig. S10)	Antisense	CDKN1A #6 (ChIP) Reverse

Primer 1 (Fig. S10)	Forward	5′-GGGTGCGGTGATGGATAAA-3′
	Reverse	5′-AGGAGAGACAGCAGAAGTCA-3′
Primer 2 (Fig. S10)	Forward	5′-AAACGGGAACCAGGACAC-3′
	Reverse	CDKN1A #6 (ChIP) Reverse
MDM2 #1 (ChIP)	Forward	5′-AGGAAGTTTCCTTTCTGGTAGG-3′
	Reverse	5′-TTCTCTGGCCAGTAAGTGATTAG-3′
MDM2 #2 (ChIP)	Forward	5′-CCGGATTAGTGCGTACGAG-3′
	Reverse	5′-TTTCGCGCTTGGAGTCG-3′
MDM2 #3 (ChIP)	Forward	5′-GGAAATCTCTGAGAAAGCCAAAC-3′
	Reverse	5′-CTCAACACATGACTCTCTGGAA-3′
MDM2 #4 (ChIP)	Forward	5′-AAGTGATCTGCCCGTCTT-3′
	Reverse	5′-CCCTGAGAAATAAATGAAATTCACC-3′
MDM2 #5 (ChIP)	Forward	5′-CCTCCCAAGTAGCTGTGTTATTT-3′
	Reverse	5′-GCCTGTAATCCCAGCACTTT-3′
SMAD3 #1 (ChIP)	Forward	5′-GGGAGGCAGCAAGAGAAAG-3′
	Reverse	5′-ACAACAAACCAATTGGCACAT-3′
SMAD3 #2 (ChIP)	Forward	5′-GTCCATCCTGCCTTTCACTC-3′
	Reverse	5′-GAGTTTCTTGACCAGGCTCTT-3′
SMAD3 #3 (ChIP)	Forward	5′-GCTCCCTCATGTCATCTACTG-3′

	Reverse	5′-CAGACCTCGTCCTTCTTCATATT-3′
SMAD3 #4 (ChIP)	Forward	5′-GACTCTTTCTCAACACAGCTAATTG-3′
	Reverse	5′-CTACTCTGGAGGTAAGTGAGGA-3′
SMAD3 #5 (ChIP)	Forward	5′-ATTAGTGGAAGGCCCAGATTT-3′
	Reverse	5′-GGGAGAAAGAGCTATTGGAGAC-3′
KLF5 #1 (ChIP)	Forward	5′-CTGTCTAATGGTATATTGTGTGTCAAC-3′
	Reverse	5′-AGGAAACCACTTCCCTTAATCC-3′
KLF5 #2 (ChIP)	Forward	5′-AGAGCCTGAGAGCACGGT-3′
	Reverse	5′-ACAGCGGCAGGCAGTTT-3′
KLF5 #3 (ChIP)	Forward	5′-AAATGATCTCTCCTGGTCTGTTC-3′
	Reverse	5′-ACCTAAGGAAGCTGATTGCC-3′
KLF5 #4 (ChIP)	Forward	5′-CAAGTACACCTAGAACCTACATCTT-3′
	Reverse	5′-GAAGCAGGACAATCCCTTGA-3′
KLF5 #5 (ChIP)	Forward	5′-CCTCCCAAAGTACTGGGATTAC-3′
	Reverse	5′-GAAGGTGGGTAGATCACTTGAG-3′
CDKN1A (Nascent RNA RT)	Antisense	5′-AAACAGGTGCAGGCTATGGGACAA-3′
SMAD3 (Nascent RNA RT)	Antisense	5′- CTACTCTGGAGGTAAGTGAGGA -3′
KLF5 (Nascent RNA RT)	Antisense	5′- GAAGCAGGACAATCCCTTGA -3′
CDKN1A #1 (Nascent RNA qPCR)	Forward	5′-TGTCCTTTCCCTTCAGTACCCTCT-3′

	Reverse	5′-TAGGGTGCCCTTCTTCTTGTGTGT-3′
CDKN1A #2 (Nascent RNA qPCR)	Forward	5′-TGGCAGTAGAGGCTATGGA-3′
	Reverse	5′-AAACGGGAACCAGGACAC-3′
CDKN1A #3 (Nascent RNA qPCR)	Forward	5′-CCTCTGCAAAGATCACCAAT-3′
	Reverse	5′-CCAGTTGCTCCATAACCTTGCC-3′
CDKN1A #4 (Nascent RNA qPCR)	Forward	5′-TCCAGGGTGACAGTGAGATT-3′
	Reverse	5′-CTCCCAAAGTGCTGGGATTATAG-3′
CDKN1A #5 (Nascent RNA qPCR)	Forward	5′-TGCACAGGGCAGAGCTTTCTACTA-3′
	Reverse	5′-AAACAGGTGCAGGCTATGGGACAA-3′
MDM2 #1 (Nascent RNA qPCR)	Forward	5′-GTGTGTAGGTCTGTAGGCTTATG-3′
	Reverse	5′-ATGTAATTCAGCATCCACCCA-3′
MDM2 #2 (Nascent RNA qPCR)	Forward	5′-TGATGGTAACCACAAGTTGTTAATG-3′
	Reverse	5′-CTGGTGCTTTCAGATATCTACCTC-3′
MDM2 #3 (Nascent RNA qPCR)	Forward	5′-CCAACCACACCTGGCTAAT-3′
	Reverse	5′-CGCCTGTAATCCCAGTACTTT-3′
MDM2 #4 (Nascent RNA qPCR)	Forward	5′-AAGTGATCTGCCCGTCTT-3′
	Reverse	5′-CCCTGAGAAATAAATGAAATTCACC-3′
SMAD3 #1 (Nascent RNA qPCR)	Forward	5′-GCTCCCTCATGTCATCTACTG-3′
	Reverse	5′-CAGACCTCGTCCTTCTTCATATT-3′

SMAD3 #2 (Nascent RNA qPCR)	Forward	5′-ACAGGAGATGTAGGGAGAAGAA-3′
	Reverse	5′-CTCTAGCCAAGTCACACAGTAAG-3′
SMAD3 #3 (Nascent RNA qPCR)	Forward	5′-TCAATGGGTGTATCTCGCTATTC-3′
	Reverse	5′-GTTGGGTTGGTGTCATTCATTT-3′
SMAD3 #4 (Nascent RNA qPCR)	Forward	5′-GAGTTTGAGACCAGCCTAGC-3′
	Reverse	5′-TTCAAGCGATTCTCCCATCTC-3′
KLF5 #1 (Nascent RNA qPCR)	Forward	5′-AAATGATCTCTCCTGGTCTGTTC-3′
	Reverse	5′-ACCTAAGGAAGCTGATTGCC-3′
KLF5 #2 (Nascent RNA qPCR)	Forward	5′-CAGAAGAAGAATGGATTGTATGTCAAG-3′
	Reverse	5′-AACCCACACATTTGTTCAATGG-3′
KLF5 #3 (Nascent RNA qPCR)	Forward	5′-AATACACAGTGAGACACAGTAA-3′
	Reverse	5′-GTAGCATTTGCTTCCTTAAGTT-3′
KLF5 #4 (Nascent RNA qPCR)	Forward	5′-GATTATCCTGTCTCAGCATCCC-3′
	Reverse	5′-CGTGAATTATGACTCCCTTTATGC-3′

Table 2-1. Primers used in Chapter 2

3. RESULTS

1. AKT phosphorylates H3 threonine 45 on DNA damage

We screened for key phosphorylation sites on core histones weather these sites were reacting by DNA-damaging agent, Adriamycin (Figure 2-1 A). In good agreement with previous report (36), DNA-damage marker H2A.X Ser139 phosphorylation was greatly increased by Adriamycin treatment. On the contrary, mitogenic specific marker H3 Thr3, 11, and Ser10, 28 were decreased. There were no apparent changes on H2A/H4 Ser1 and H2B Ser36, while H3 Thr45 phosphorylation dramatically increased by Adriamycin treatment.

Comparing H3-T45 phosphorylation with γH2AX induction by confocal microscopy, we found that the induction fold of H3-T45 phosphorylation was not greater than that of γH2AX (Figure 2-1 B). Unlike H2AX phosphorylation which is barely seen in normal condition and greatly induced under DNA damaging conditions, phosphorylation of H3-T45 resides at low level even under normal conditions. However, unlike γH2AX which formed speckled foci on DNA double strand break sites, H3-T45 phosphorylation showed more broad, nuclear-wide distribution (Figure 2-1 C).

Careful inspection of the amino acid sequence of core histones, we observed well-conserved AKT substrate motifs on histone H2B and H3 (Figure 2-1 D). Even though it has been known that DNA damage-induced histone phosphorylation is related to regulate the chromatin states, the link between

DNA damage-activated AKT and chromatin states is still obscure. Thus, we determine whether this site was phosphorylated by AKT on DNA damage.

In MCF10A normal breast epithelial cells, phosphorylation of both AKT and H3-T45 increased with etoposide (ETPS), adriamycin (ADR), and UV exposure (Figure 2-1 E and F). AKT inhibitor IV is a cell-permeable drug that targets an ATP-binding site of a kinase that is immediately upstream of AKT but downstream of PI3K, thereby specifically inhibiting AKT phosphorylation (37). The enhanced phosphorylation of AKT and H3-T45 with ADR treatment was mitigated by AKT inhibitor IV (Figure 2-1 G). And dose dependent increase of adriamycin or AKT inhibitor IV treatment affected both AKT and H3-T45 phosphorylation (Figure 2-1 H and I)

Figure 2-1.

A

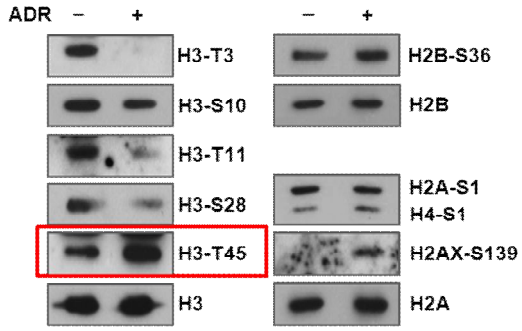

B

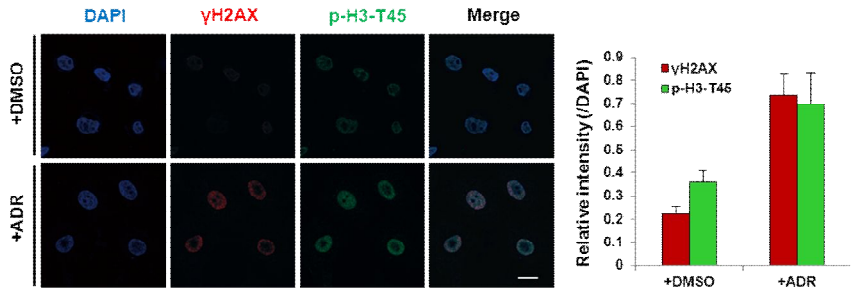

C

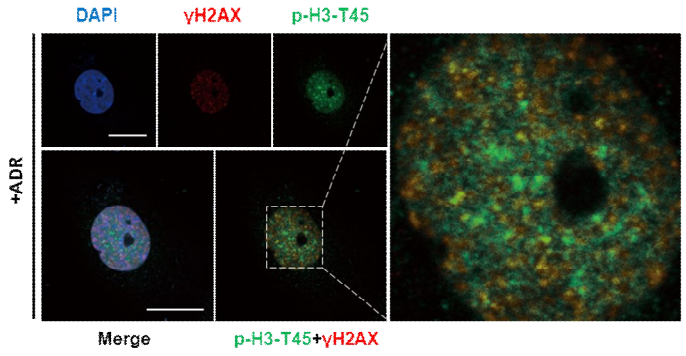

D

AKT substrates :	R-X-R-X-X-S/T
GSK3 β	R P R T T S_9
PGC1 α	R S R S R S_{570}
H2B	R S R K E S_{36}
H3	R Y R P G T_{45}

Figure 2-1.

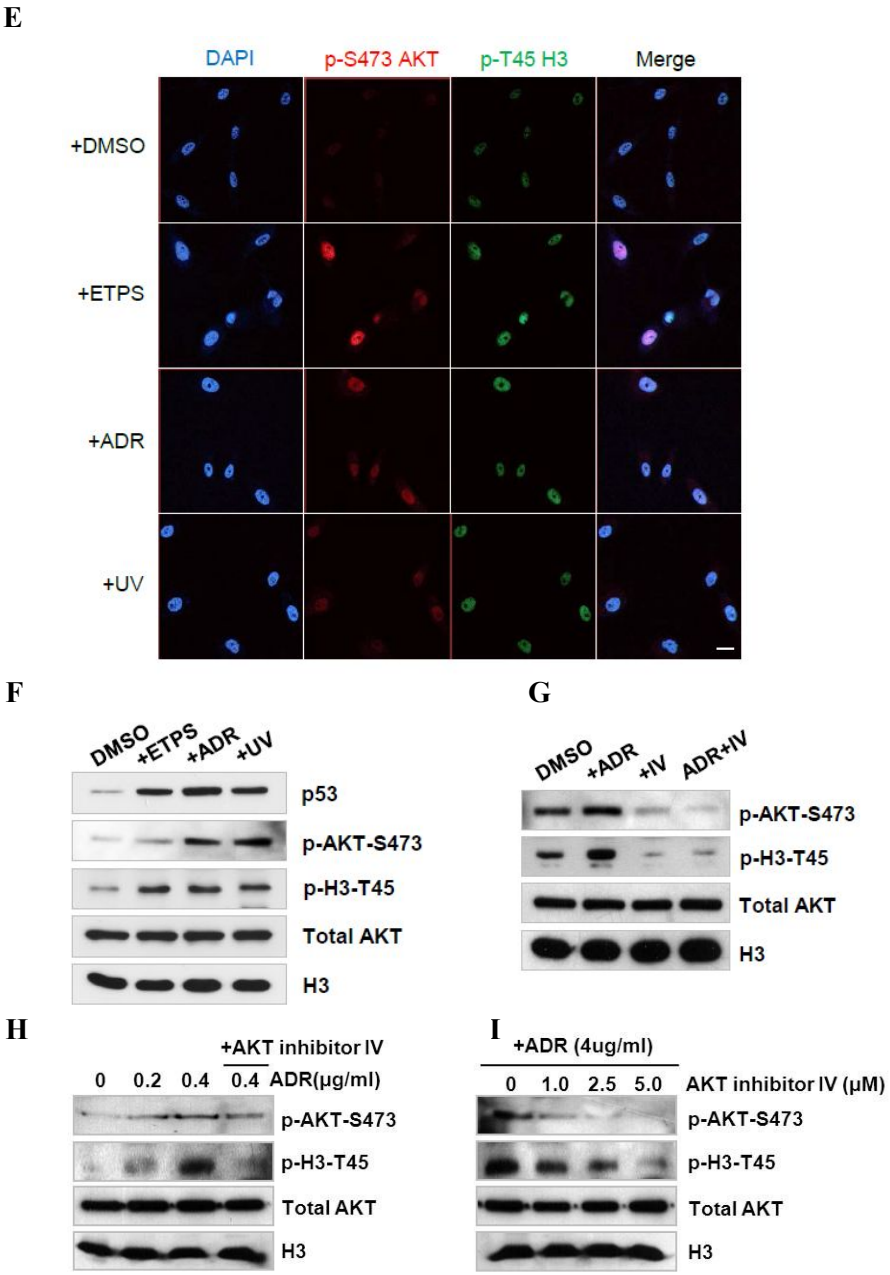

Figure 2-1. AKT phosphorylates H3 threonine 45 on DNA damage.

(**A**) MCF10A normal breast epithelial cells were treated with DMSO (-) or 0.4 μg/ml ADR for 18 hours. Total cell lysates were probed for western blot with

indicated antibodies. (**B**) MCF10A cells, growing on coverslips were treated with 0.4 μg/ml ADR 18 hours. Cells were fixed, permeabilized, stained with anti-phosphorylated H3-T45 (green) and γH2AX (red). DNA counterstained with DAPI. Signal intensity of both signals was compared. Standard deviations are indicated as error bars ($n \geq 3$). (**C**) Co-localization of H3-T45 (green) and γH2AX (red), in higher resolution data of a single MCF10A cell in (A). Scale bars 10 μm. (**D**) AKT substrate sequences conserved in various proteins, including histone H2B and H3. (**E**) Immunofluorescence staining of phosphorylated AKT-serine 473 (p-AKT-S473) and phosphorylated H3-threonine 45 (p-H3-T45) in MCF10A cells. Cells were treated with DMSO, 100 μM etoposide (ETPS), 0.4 μg/ml adriamycin (ADR), or 50 J/m^2 UV irradiation (UV) for 18 hours. DNA counterstained with DAPI; scale bar, 20 μm. (**F**) Western blot of samples in (E). (**G**) MCF10A cells were treated with DMSO, 0.4 μg/ml ADR, 0.2 μM AKT inhibitor IV (IV), or 0.4 μg/ml ADR and 0.2 μM AKT inhibitor IV for 18 hours. Total cell extracts were probed by western blot. Data shown are the representative of three independent experiments. (**H**) MCF10A cells were treated with 0, 0.2, 0.4 μg/ml of ADR and 0.4 μg/ml ADR + 0.2 μM AKT inhibitor IV for 18 hours. Total cell lysates were probed for western blot. (**I**) MCF10A cells were treated with 0.4 μg/ml ADR with/without indicated concentrations of AKT inhibitor IV for 18 hours. Total cell lysates were probed for western blot.

2. AKT phosphorylates H3-T45 *in vitro* and *in vivo*

To test if AKT directly phosphorylates core histones, we performed AKT *in vitro* kinase assay using bacterially purified core histones as substrates.

Among four core histones, H2B and H3 were phosphorylated by AKT *in vitro* kinase assay (Figure 2-2 A). Using truncated mutant form of H3 as a substrate of AKT *in vitro* kinase assay, we could predict the amino acid between 36 and 51 was phosphorylated by AKT (Figure 2-2 B). And by point mutating 45^{th} threonine of H3 (Figure 2-2 C) and 36^{th} serine (Figure 2-2 D) into alanine almost completely abrogated the phosphorylation by AKT.

Direct interaction of H2B and H3 with AKT was confirmed by *in vitro* GST pulldown assay using GST-tagged bacterially purified histones (Figure 2-2 E). We generated more specific rabbit polyclonal anti-phosphorylated H3-T45 antibody for subsequent experiments.

Generated antibody successfully detected endogenous H3-T45 phosphorylation in MCF7 breast cancer cell lysates, while treating AKT inhibitor IV or blocking antibody with phosphorylated H3-T45 peptide (Figure 2-2 F) did not. And Western blot successfully detected H3 in immunoprecipitates of generated antibody (Figure 2-2 G).

H3-T45 phosphorylation reaction by AKT *in vitro* kinase assay required the cofactors for phosphorylation reaction such as ATP or magnesium (Figure 2-2

H), and not kinase activity deficient (dominant negative), but constitutively activated kinase activity (myristoylated) mutant of AKT was required for H3-T45 phosphorylation (Figure 2-2 I). *In vivo* phosphorylation of H3-T45 also required the activity of AKT itself in both MCF10A cells (Figure 2-2 J) and HeLa cells (Figure 2-2 K). Therefore, we concluded that H3-T45 is an actual substrate of AKT.

Figure 2-2.

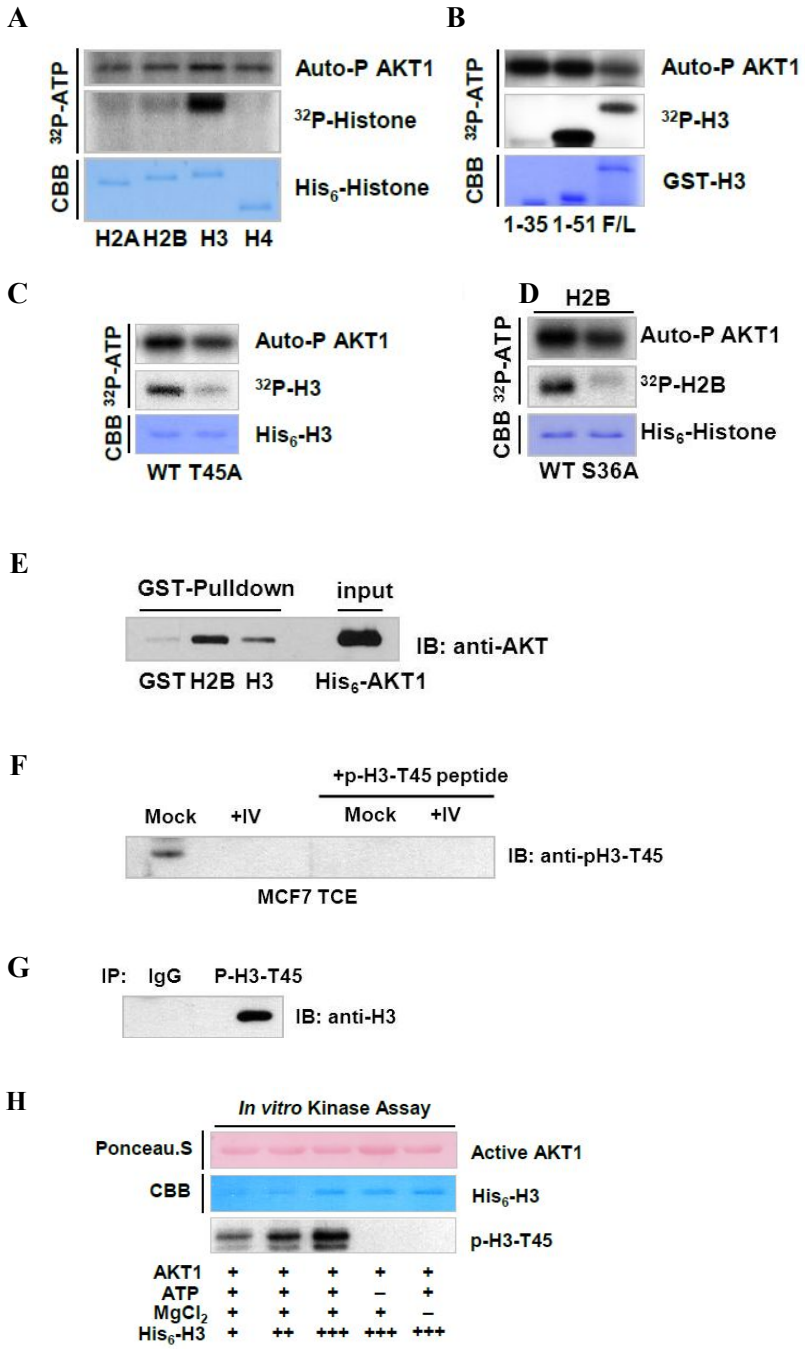
A
32P-ATP
CBB
Auto-P AKT1
32P-Histone
His6-Histone
H2A H2B H3 H4
B
32P-ATP
CBB
Auto-P AKT1
32P-H3
GST-H3
1-35 1-51 F/L
C
32P-ATP
CBB
Auto-P AKT1
32P-H3
His6-H3
WT T45A
D
H2B
32P-ATP
CBB
Auto-P AKT1
32P-H2B
His6-Histone
WT S36A
E
GST-Pulldown
input
IB: anti-AKT
GST H2B H3
His6-AKT1
F
+p-H3-T45 peptide
Mock
+IV
Mock
+IV
IB: anti-pH3-T45
MCF7 TCE
G
IP: IgG
P-H3-T45
IB: anti-H3
H
In vitro Kinase Assay
Ponceau.S
CBB
Active AKT1
His6-H3
p-H3-T45
AKT1 + + + + +
ATP + + + – +
MgCl2 + + + + –
His6-H3 + ++ +++ +++ +++

Figure 2-2.

I

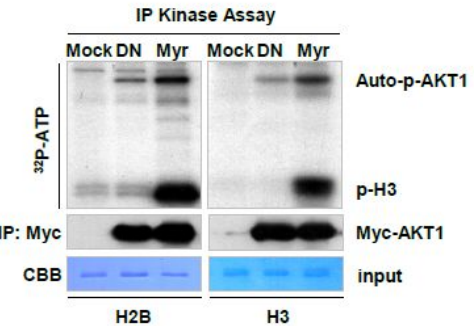

J

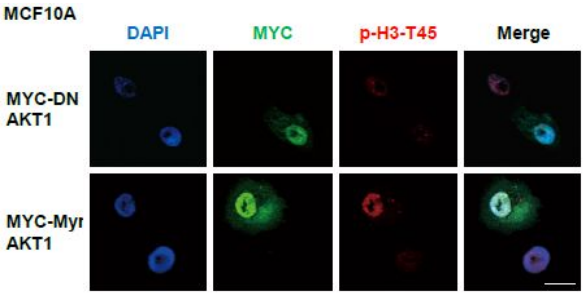

K

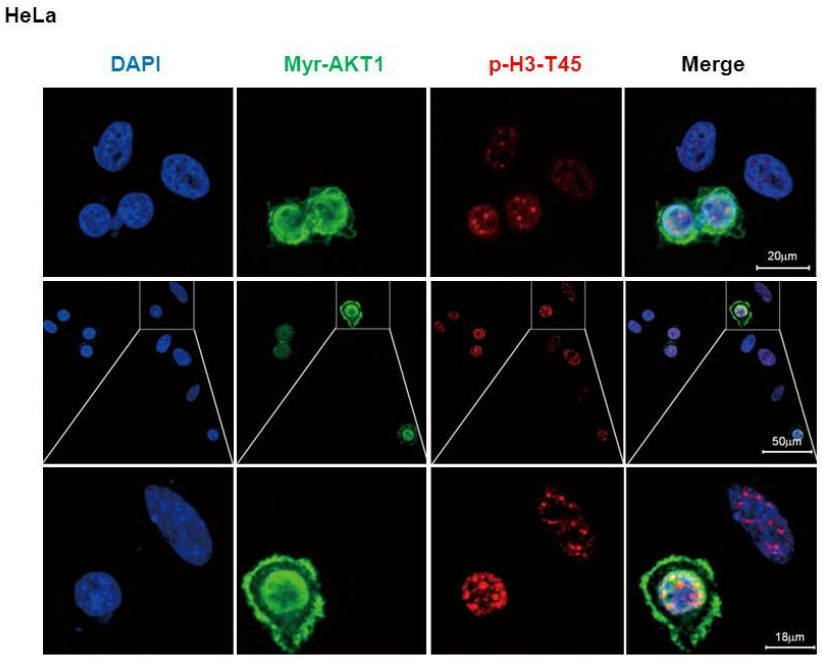

Figure 2-2. AKT1 phosphorylates H3-T45 *in vitro* and *in vivo.*

(**A**) *In vitro* kinase assay of recombinant His_6-tagged core histones purified from *E. coli*. (**B**) AKT1 *in vitro* kinase assay of His_6-H3. F/L indicates the full-length of H3. 1-35 and 1-51 represent the corresponding amino acid sequence of purified H3. (**C**) AKT1 *in vitro* kinase assay of full-length H3, wild-type (WT) and T45 mutated to alanine (T45A). Autophosphorylated AKT1 (auto-P AKT1) is shown as a kinase loading control. (**D**) AKT1 *in vitro* kinase assay of histone H2B WT and H2B ser36, mutated to alanine (S36A). (**E**) GST-pulldown assay of GST-H2B and H3, mixed with His_6-AKT1. GST histones were pulled down using glutathione sepharose bead and probed with anti-AKT antibody. (**F**) Rabbit polyclonal anti-phosphorylated H3-T45 antibody was produced. MCF7 cells were treated with DMSO or AKT inhibitor IV, total cell lysates were probed for western blot. Transferred NC membrane was incubated with anti phosphorylated H3-T45 antibody was blocked with/without phosphorylated H3-T45 peptide. (**G**) MCF7 total cell lysates were immunoprecipitated using normal rabbit IgG or anti phosphorylated H3-T45 antibody and probed for anti H3 antibody. (**H**) *In vitro* AKT1 kinase assay with/without non-radiolabeled ATP or $MgCl_2$. Assay samples were probed with anti-phosphorylated H3-T45 antibody. (**I**) IP kinase assay of Myc-tagged blank vector, dominant negative (DN), and constitutively-active myristoylated (Myr) AKT1. AKT1 constructs were transfected into HEK293T cells and cell lysates were immunoprecipitated with anti-Myc antibody, subjected to *in vitro* kinase assay. (**J**) Immunofluorescence staining for Myc-tagged DN/Myr-AKT1 overexpressed

in MCF10A. DNA counterstained with DAPI. Scale bar, 20 μm. All above data shown are the representative of three independent experiments. (**K**) Immunofluorescence staining for Myc-DN and Myr-AKT1 overexpressed in HeLa cells. DNA counterstained with DAPI. Scale bars are as indicated.

3. H3-T45 phosphorylation signal is abundant near the TTS

H3-T45 lies in the N-terminus of the first helix of H3 and constitutes the nucleosome entry/exit point. This residue is assumed to play highly important role, as it makes contact with genomic DNA (9,10,38). To examine H3-T45 phosphorylation on DNA damage, MCF10A cells were treated with ADR, and genomewide ChIP-seq was performed with anti-phosphorylated H3-T45, yielding a set of phosphorylated H3-T45-containing genes.

In our functional annotation analysis, most phosphorylated H3-T45-positive regions were cellular stress-responsive genes (Figure 2-3 A-B); the signal appeared primarily in the gene coding region, showing major abundance in the downstream areas (Figure 2-3 C). Metagene profiling analysis revealed that genomic distribution pattern of phosphorylated H3-T45 showed major abundance in 3' of gene TTS (Figure 2-3 D). And adriamycin treatment clearly induced H3-T45 phosphorylation on TTS (Figure 2-3 E).

The specific pattern of H3-T45 phosphorylation, which showed major distribution around TTS, resembles that of phosphorylated RNA polymerase II CTD-Ser2 (PolII-S2) / transcription termination factors (25,39). In comparing ChIP-seq profiles, we noted that over 67% of H3-T45 phosphorylation overlapped with RNA PolII-S2 phosphorylation (Figure 2-3 F). Inspection of individual DNA-damage responsive genes by IGV agreed with our finding that H3-T45 phosphorylation resembling RNA PolII-S2 phosphorylation (Figure 2-3 G). Housekeeping genes, such as *GAPDH* and

HPRT1, were phosphorylated H3-T45-negative (Figure 2-3 H), which showed lower RNA PolII-S2 phosphorylation levels than H3-T45 positive genes (Figure 2-3 G and H; RNA PolII-S2 scale data ranges are 21 and 19 on *CDKN1A* and *MDM2* versus 7.3 and 2.9 on *GAPDH* and *HPRT1*, respectively).

Inspection of *CDKN1A* gene locus by ChIP-qPCR well recapitulated genomewide ChIP-seq. Phosphorylated H3-T45 signals in *CDKN1A* rose significantly on induction of *CDKN1A* transcription by ADR, peaking 3' of the TTS, where RNA PolII separated from the chromatin (Figure 2-3 I and J). In good agreement with the ChIP-Seq data, not only the phosphorylation pattern of H3-T45 in *CDKN1A*, but also in *MDM2*, *SMAD3*, and *KLF5* gene locus also showed highly similar pattern with RNA PolII-S2 phosphorylation (Figure 2-3 K). Moreover, the AKT occupancy on the TTS of *CDKN1A* was significantly increased by adriamycin treatment while AKT occupancy on the promoter of *CDKN1A* was not affected (Figure 2-3 L and M).

CDC7, PKC-δ, and DYRK1A are previously known to phosphorylate H3-T45 (9,10,40). So, we tested whether these kinases affect H4-T45 phosphorylation under DNA damaging condition. Adriamycin treatment induced overall H3-T45 phosphorylation and PKC-δ knockdown slightly enhanced its induction (Figure 2-3N and O). However, H3-T45 phosphorylation occupying on the TTS of *CDKN1A*, *MDM2*, *SMAD3*, and

KLF5 was not significantly affected by PKC-δ, CDC7 and DYRK1A knockdown (Figure 2-3 P).

Taken together, these data suggest that DNA damage-induced H3-T45 phosphorylation occurs exclusively 3' of the TTS in actively transcribed genes, where RNA PolII-S2 phosphorylation is maximized.

Figure 2-3.

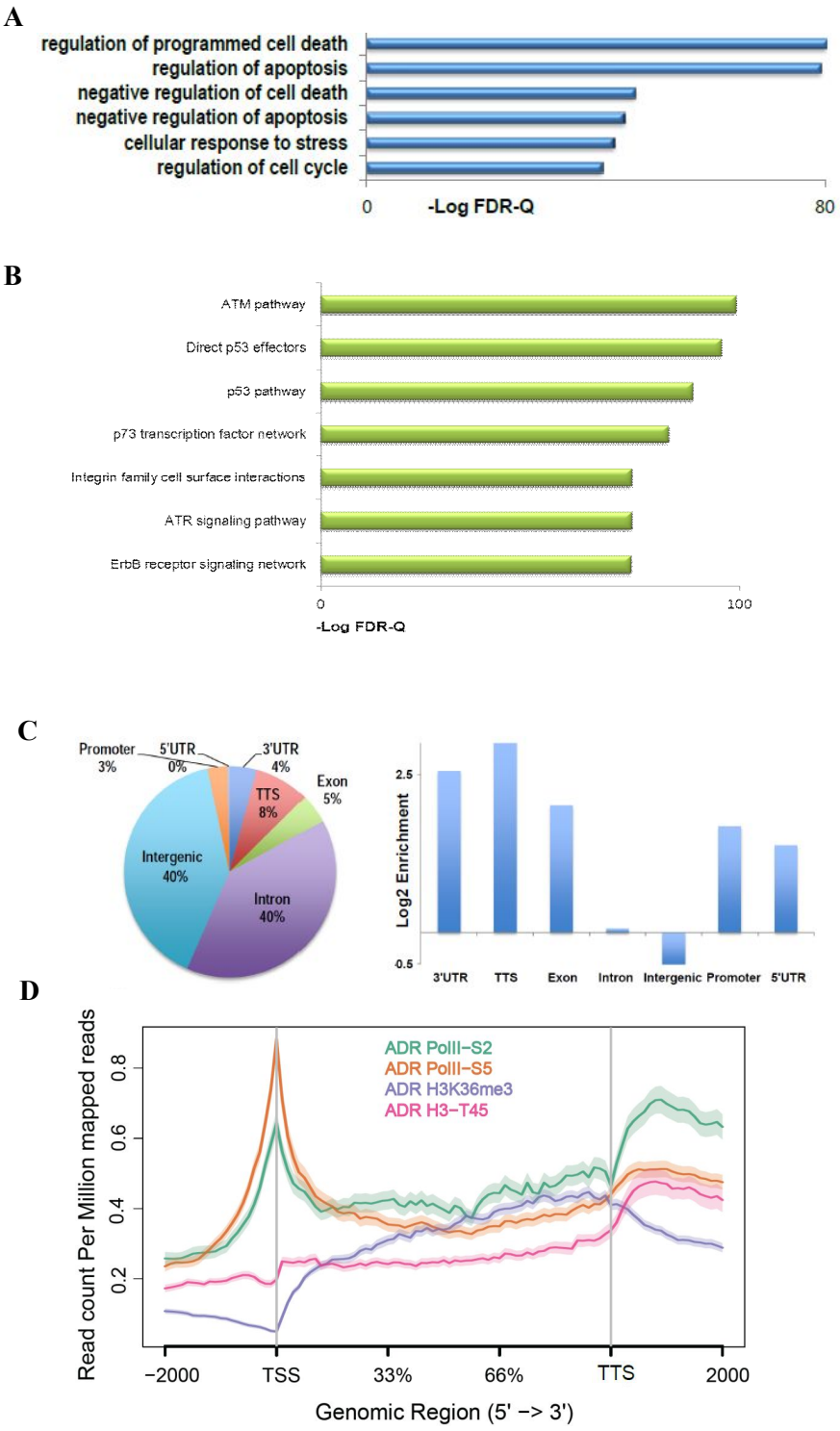
A
regulation of programmed cell death
regulation of apoptosis
negative regulation of cell death
negative regulation of apoptosis
cellular response to stress
regulation of cell cycle
0
-Log FDR-Q
80
B
ATM pathway
Direct p53 effectors
p53 pathway
p73 transcription factor network
Integrin family cell surface interactions
ATR signaling pathway
ErbB receptor signaling network
0
100
-Log FDR-Q
C
Promoter 3%
5'UTR 0%
3'UTR 4%
Exon 5%
TTS 8%
Intergenic 40%
Intron 40%
Log2 Enrichment
2.5
-0.5
3'UTR
TTS
Exon
Intron
Intergenic
Promoter
5'UTR
D
ADR PolII-S2
ADR PolII-S5
ADR H3K36me3
ADR H3-T45
Read count Per Million mapped reads
0.2
0.4
0.6
0.8
-2000
TSS
33%
66%
TTS
2000
Genomic Region (5' -> 3')

Figure 2-3.

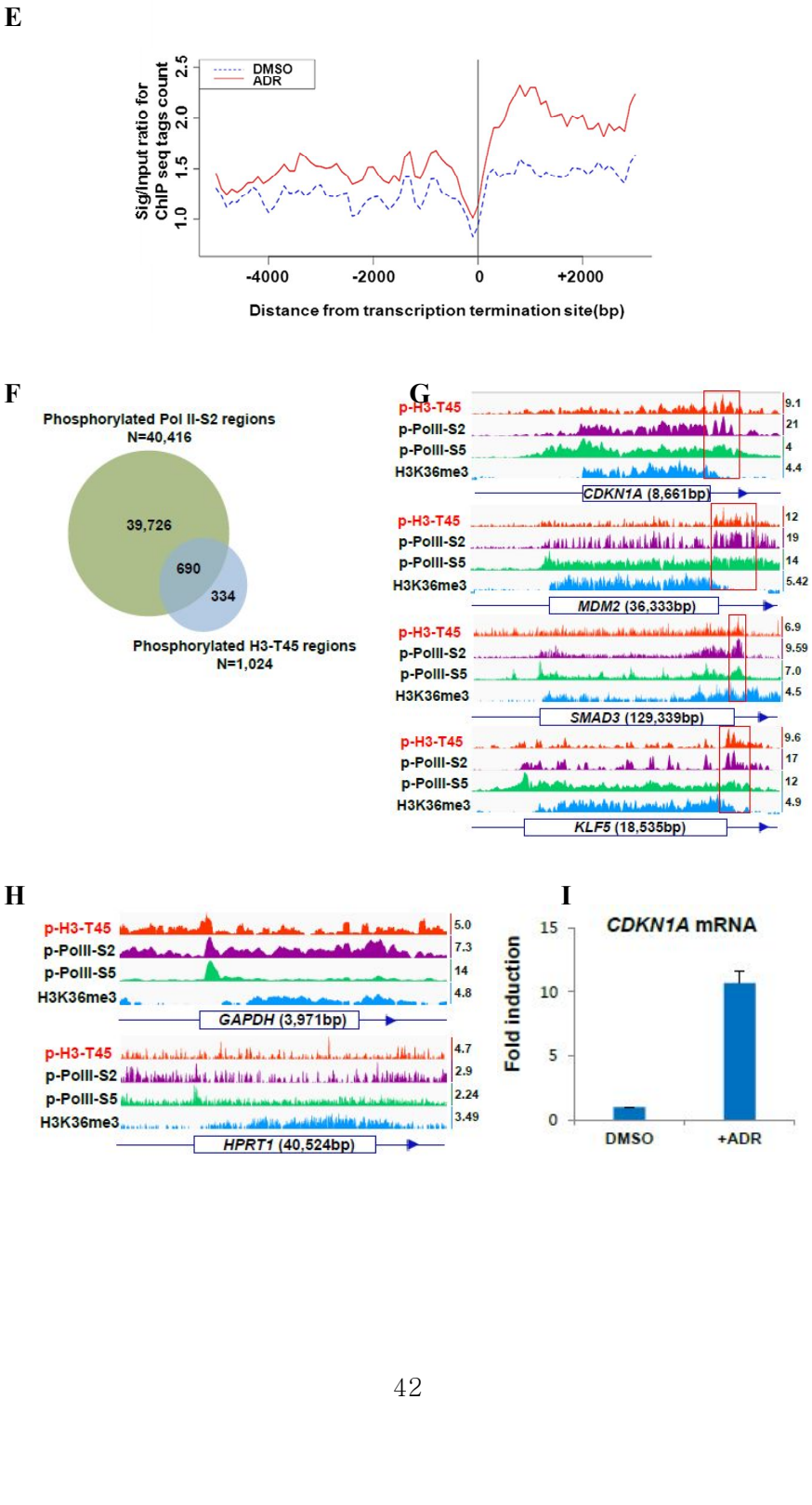
E
DMSO
ADR
Sig/Input ratio for ChIP seq tags count
1.0
1.5
2.0
2.5
-4000
-2000
0
+2000
Distance from transcription termination site(bp)
F
Phosphorylated Pol II-S2 regions
N=40,416
39,726
690
334
Phosphorylated H3-T45 regions
N=1,024
G
p-H3-T45
p-PolII-S2
p-PolII-S5
H3K36me3
9.1
21
4
4.4
CDKN1A (8,661bp)
12
19
14
5.42
MDM2 (36,333bp)
6.9
9.59
7.0
4.5
SMAD3 (129,339bp)
9.6
17
12
4.9
KLF5 (18,535bp)
H
5.0
7.3
14
4.8
GAPDH (3,971bp)
4.7
2.9
2.24
3.49
HPRT1 (40,524bp)
I
CDKN1A mRNA
Fold induction
15
10
5
0
DMSO
+ADR

Figure 2-3.

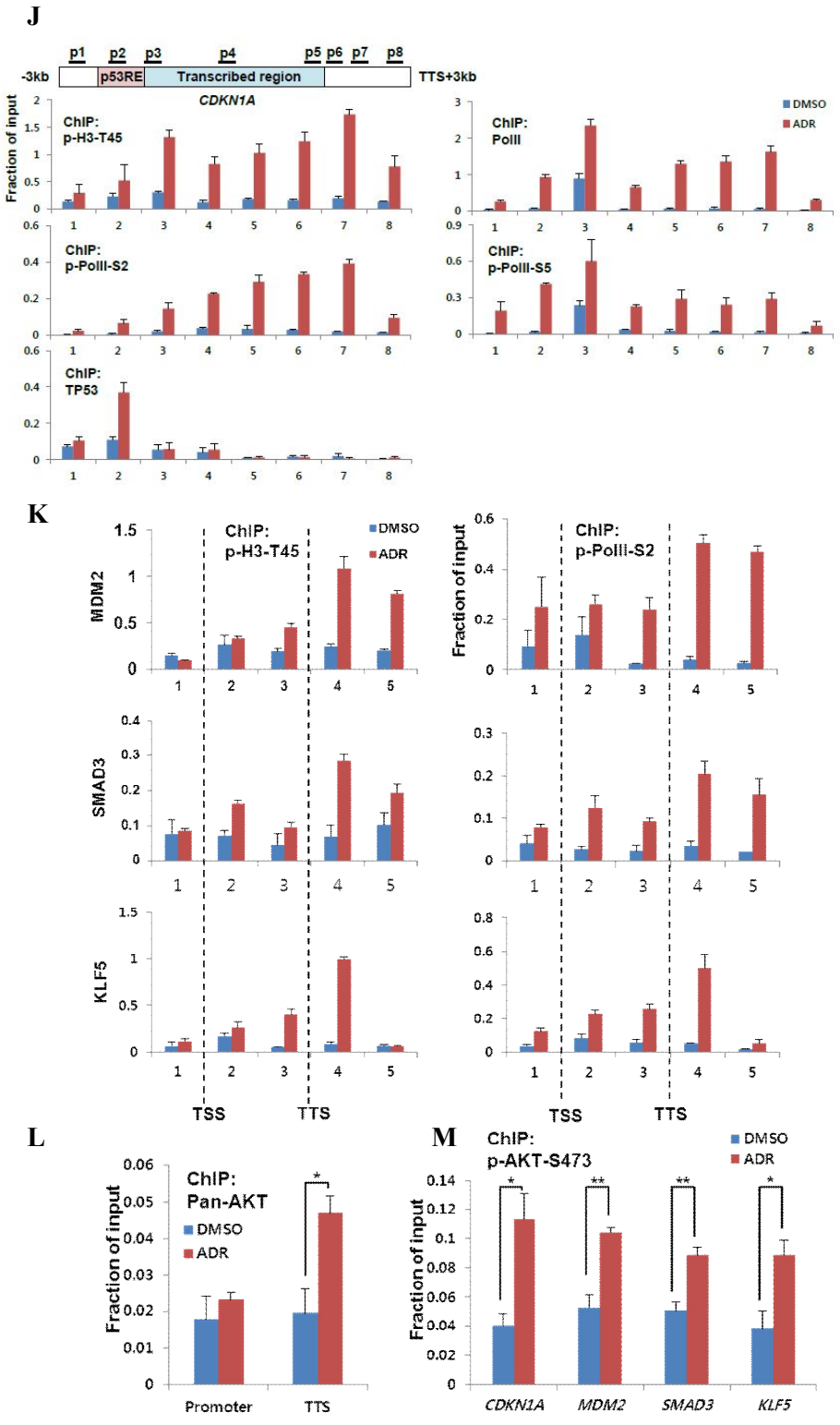
J
p1
p2
p3
p4
p5
p6
p7
p8
-3kb
p53RE
Transcribed region
TTS+3kb
CDKN1A
Fraction of input
ChIP:
p-H3-T45
ChIP:
PolII
DMSO
ADR
ChIP:
p-PolII-S2
ChIP:
p-PolII-S5
ChIP:
TP53
K
ChIP:
p-H3-T45
DMSO
ADR
ChIP:
p-PolII-S2
MDM2
SMAD3
KLF5
TSS
TTS
L
ChIP:
Pan-AKT
DMSO
ADR
Fraction of input
Promoter
TTS
M
ChIP:
p-AKT-S473
DMSO
ADR
Fraction of input
CDKN1A
MDM2
SMAD3
KLF5

Figure 2-3.

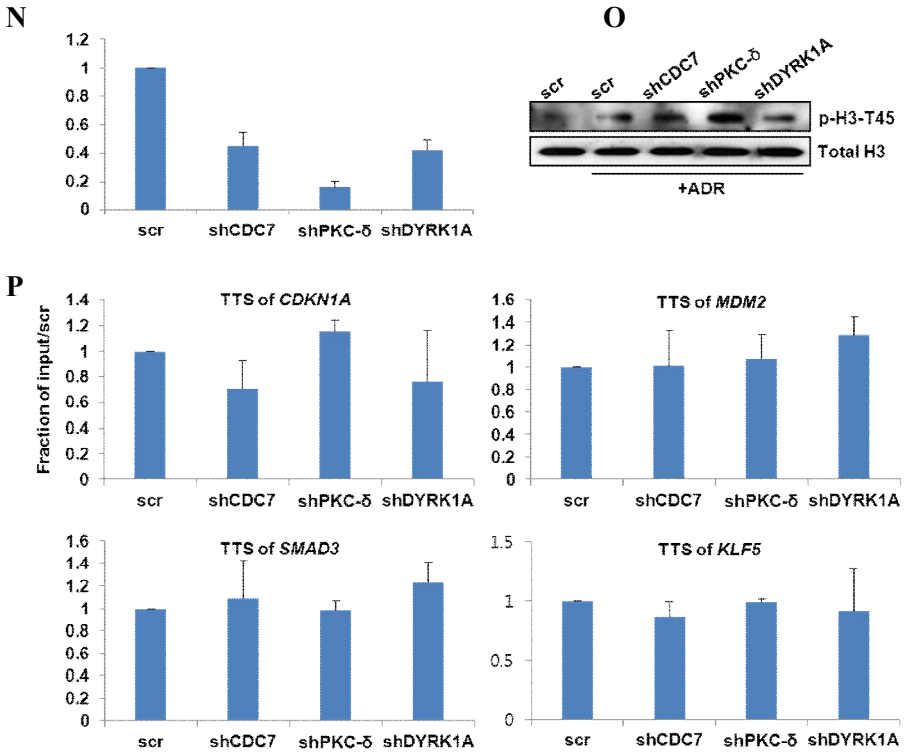

Figure 2-3. H3-T45 phosphorylation signal is abundant near the TTS.

MCF10A cells were treated with 0.4 μg/ml ADR for 18 hours and analyzed by ChIP-seq. (**A**) Functional annotation of H3-T45 phosphorylation peak. (**B**) MCF10A cells were treated with 0.4 μg/ml ADR for 18 hours and analyzed by ChIP-seq. Functional annotation (biological pathway) analysis of H3-T45 phosphorylation peak. (**C**) Pie chart showing the proportion of transcript coordinates for H3-T45 phosphorylation peaks (1041 regions). Proportion of transcript coordinates for H3-T45 phosphorylation peaks were compared to RefSeq transcripts. (**D**) Average profiles for phosphorylated PolII-S2, S5, H3K36me3, and phosphorylated H3-T45 were plotted around ADR induced H3-T45 phosphorylation enriched genes (610 genes) (**E**) Average profiles for

phosphorylated H3-T45 were plotted around DMSO and ADR induced H3-T45 phosphorylation enriched genes. (**F**) Phosphorylated RNA PolII-S2 and phosphorylated H3-T45 ChIP peak distribution. (**G**), (**H**) ChIP binding profiles of indicated genes. Scale data ranges are indicated on the right side of the individual track. Red boxes indicate the highest peak of phosphorylated H3-T45 signal. (**I**) Real-time qPCR analysis of *CDKN1*A mRNA in DMSO/ADR-treated MCF10A cells. (**J**) ChIP assay covering the *CDKN1A* locus above with indicated antibodies. Values were normalized with 1% input DNA. Real-time qPCR and ChIP assay data shown are the average value of at least three independent experiments. Standard deviations are indicated as error bars. (K) ChIP-qPCR of indicated gene locus with anti-phosphorylated H3-T45 and anti-phosphorylated RNA Pol II-S2. (L) ChIP-qPCR of promoter and TTS of *CDKN1A,* using anti-pan AKT. (M) ChIP-qPCR using anti-phosphorylated AKT-S473. qPCR was performed with primers complement to the TTS locus of indicated genes. (**N**) Real-time qPCR analysis of corresponding mRNAs in lentivirus mediated CDC7, PKC-δ, and DYRK1A knockdown MCF10A cells. (**O**) MCF10A cells were treated with/without 0.4 μg/ml ADR for 18 hours. Whole cell lysates were probed for Western blot with indicated antibodies. (**P**) ChIP assay was performed using anti-phosphorylated H3-T45 in ADR treated MCF10A cells, analyzed with qPCR using primers complement to the TTS of indicated genes. Values were normalized with 1% input DNA/scr. Standard deviations are indicated as error bars.ChIP-pPCR values were normalized with 1% input DNA. Real-time

qPCR and ChIP assay data shown are the average value of at least three independent experiments. Standard deviations are indicated as error bars. * $p<0.05$, ** $p<0.001$

4. AKT1 phosphorylates H3-T45 phosphorylation more efficiently than AKT2.

In human cells, 3 genes (*AKT1*, *AKT2* and *AKT3*), on chromosomes 14, 19, and 1, respectively, encode distinct AKT proteins. Only AKT1 and AKT2 are ubiquitously expressed in all tissue types, while AKT3 is tissue and cell type specific (41).

To determine the AKT isoforms that mediate H3-T45 phosphorylation, we generated AKT1 and AKT2 knockdown MCF10A cells. Successful knockdown of AKTs were confirmed by both realtime PCR and western blot analysis (Figure 2-4 A and B).

By ChIP-qPCR, knockdown of AKT1 suppressed H3-T45 phosphorylation by ADR (Figure 2-4 C). The level of *CDKN1A* mRNA was consistent with the ChIP-qPCR results, showing significantly retarded expression by AKT1 knockdown (Figure 2-4 D). In contrast, AKT2 knockdown had a moderate effect in inhibiting H3-T45 phosphorylation and *CDKN1A* transcription. Consistent with *CDKN1A* mRNA, *MDM2*, *SMAD3*, and *KLF5* mRNA levels were significantly decreased by AKT1 knockdown (Figure 2-4 E). From these data, we concluded that AKT1 is the major kinase phosphorylating H3-T45 upon DNA damage.

Figure 2-4.

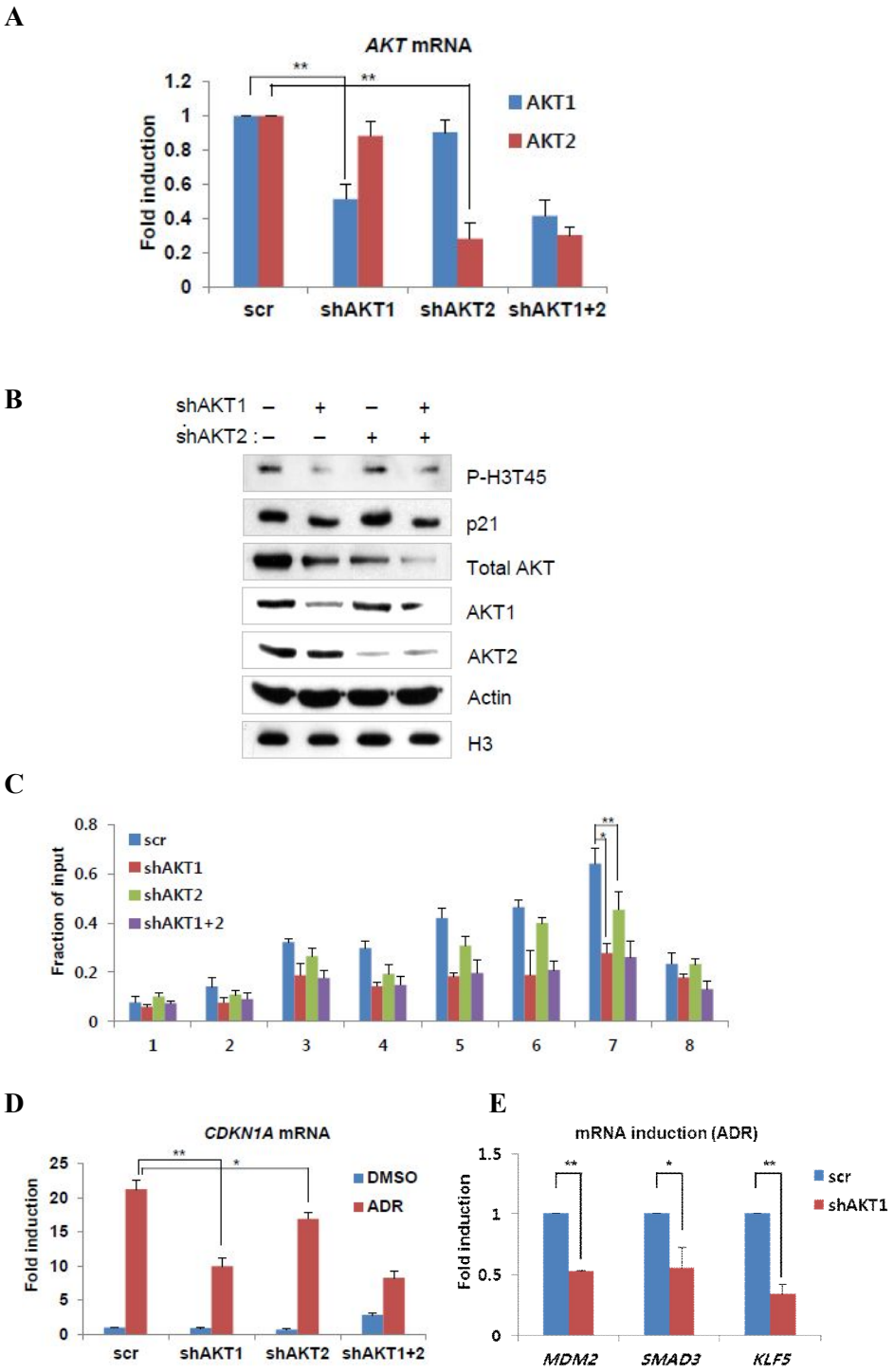
A
AKT mRNA
Fold induction
AKT1
AKT2
scr
shAKT1
shAKT2
shAKT1+2
B
shAKT1
shAKT2
P-H3T45
p21
Total AKT
AKT1
AKT2
Actin
H3
C
Fraction of input
scr
shAKT1
shAKT2
shAKT1+2
D
CDKN1A mRNA
Fold induction
DMSO
ADR
E
mRNA induction (ADR)
Fold induction
scr
shAKT1
MDM2
SMAD3
KLF5

Figure 2-4. AKT1 phosphorylates H3-T45 phosphorylation more efficiently than AKT2.

(**A**) Real-time PCR analysis of *AKT* mRNA. (**B**) Western blot analysis of total cell extracts with indicated antibodies. (**C**) Phosphorylated H3-T45 ChIP assay of the *CDKN1A* locus. (**D**) Real-time PCR analysis of *CDKN1A* mRNA. (**E**) mRNA real-time PCR analysis of indicated genes from ADR treated MCF10A cells. Real-time PCR and ChIP assay data shown are the average value of at least three independent experiments. Standard deviations are indicated as error bars. $*p<0.05$, $**p<0.001$.

5. H3-T45 phosphorylation is critical for the transcription termination.

To examine the effects of H3-T45 phosphorylation on transcription termination, we generated MCF10A cells that stably overexpressed a phosphorylation-defective mutant of H3-T45 (T45A) (Figure 2-5 A). Despite the residual endogenous H3, the T45A mutation and AKT inhibitor IV suppressed ADR-induced *CDKN1A* transcription (Figure 2-5 B).

To determine whether AKT inhibitor IV treatment or the T45A mutation affected 3'-end processing, which is a crucial step in transcription termination (39), total RNA was reverse-transcribed with a complementary primer that encompassed the 3' region of *CDKN1A* (Figure 2-5 C). This primer generates 2 complementary DNAs (cDNAs): a long, uncleaved pre-mRNA transcript and a shorter transcript that results from cleavage at the poly(A) site. The cDNA was analyzed with primer pairs to 3 regions: 1) the last intronic region, amplifying pre-mRNA (not mature mRNA), 2) the poly(A) site, to detect uncleaved pre-mRNA product, and 3) the downstream RNA after cleavage at the poly(A) site, generating a product that lacks a 5' cap and is degraded rapidly by exonucleases.

In DMSO- and ADR-treated cells, the amounts of PCR products 1 and 3 were similar, despite the induction of pre-mRNA (Figure 2-5 D). However, the downstream RNA product increased in AKT inhibitor-treated cells and T45A mutant cells. The amount of product 2 was not altered by AKT

inhibition or the T45A mutation, indicating that inhibition of AKT and the T45A mutation affect the degradation of downstream RNA products after poly(A) site cleavage but not cleavage of the mRNA proper.

To analyze the effect of H3-T45 phosphorylation on RNA transcripts more quantitatively, we used nascent RNA capture system. 5-ethynyl uridine (EU) was treated into the culture medium with adriamycin. 18 hours-post treatment, total RNA was purified, and EU-labeled RNAs were biotinylated using copper-catalyzed cycloaddition reaction (click chemistry). Biotinylated RNAs were than further purified with streptavidine coated magnetic beads, washed, reverse-transcribed, and analyzed with realtime-qPCR with specific primers. As a result, we could observe significantly increased 3' RNAs downstream poly(A) site (Figure 2-5 E). In good agreement with Figure 2-5 D, these data indicate that the 3' end processing of DNA damage response genes were affected by H3-T45 phosphorylation.

By checking RNA PolII occupancy by ChIP-qPCR analysis, we could observe the increased RNA PolII distribution downstream TTS regions of DNA damage response genes in the T45A mutant, demonstrating that the T45A mutation impairs transcription termination (Figure 2-5 F).

Figure 2-5.

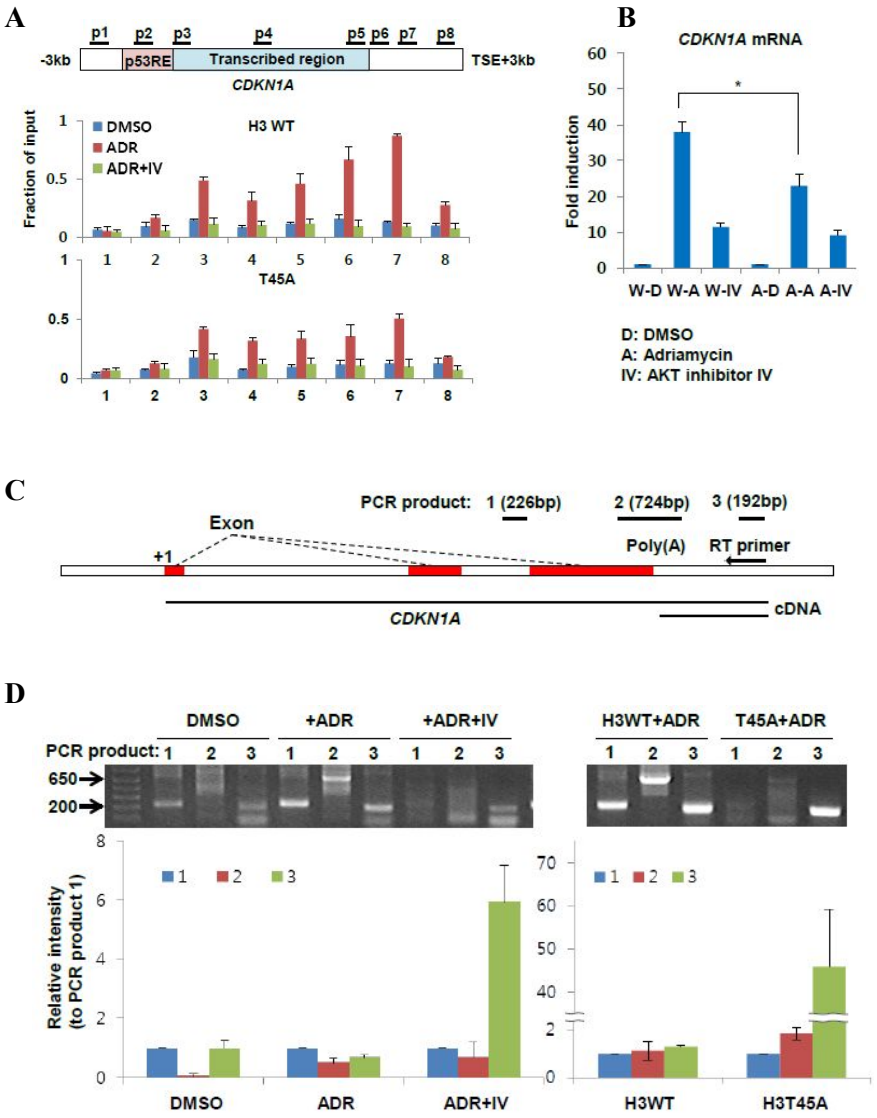
A
p1 p2 p3 p4 p5 p6 p7 p8
-3kb
p53RE
Transcribed region
TSE+3kb
CDKN1A
Fraction of input
DMSO
ADR
ADR+IV
H3 WT
T45A
B
CDKN1A mRNA
Fold induction
W-D W-A W-IV A-D A-A A-IV
D: DMSO
A: Adriamycin
IV: AKT inhibitor IV
C
PCR product: 1 (226bp) 2 (724bp) 3 (192bp)
Exon
+1
Poly(A)
RT primer
CDKN1A
cDNA
D
DMSO +ADR +ADR+IV
H3WT+ADR T45A+ADR
PCR product: 1 2 3
650
200
Relative intensity
(to PCR product 1)
DMSO ADR ADR+IV
H3WT H3T45A

Figure 2-5.

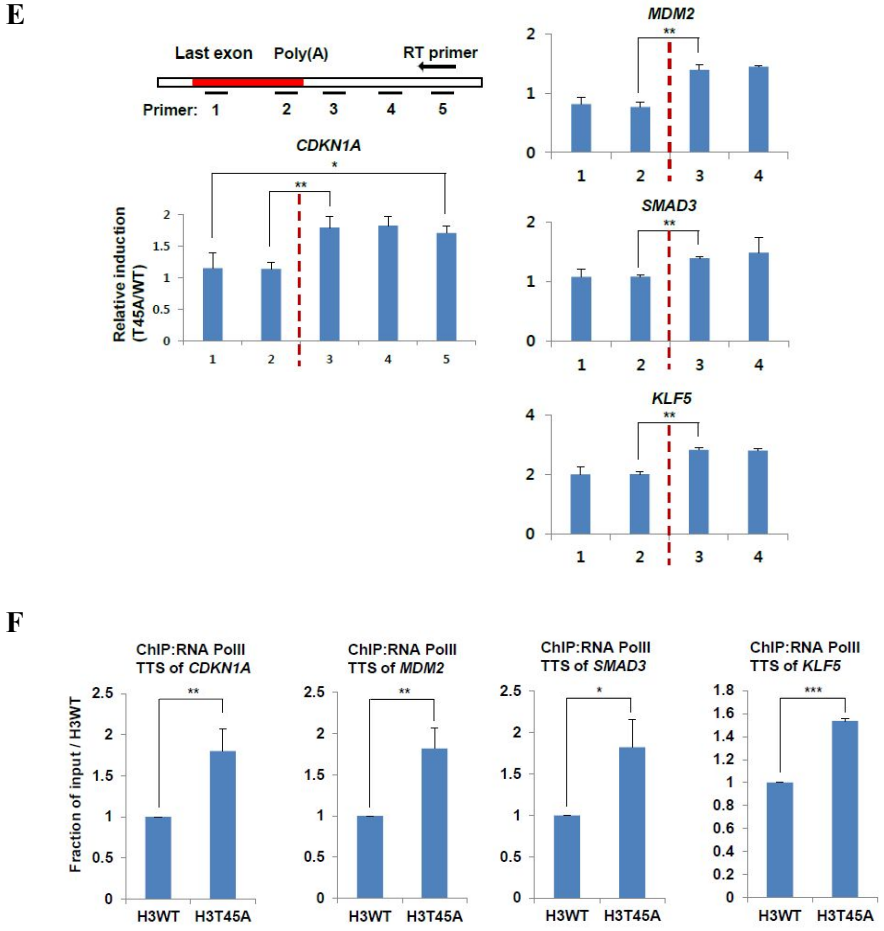

Figure 2-5. H3-T45 phosphorylation is critical for transcription termination.

(**A**) ChIP assay of phosphorylated H3-T45 from H3 WT or T45A mutant overexpressing MCF10A cells. (**B**) Real-time qPCR of *CDKN1A* mRNA in cells from (A) prior to crosslinking. (**C**) Schematic of *CDKN1A* locus. (**D**) PCR reaction of products in (C). MCF10A cells and H3 WT or T45A mutant-overexpressing cells were treated with the indicated drugs for 18 hours, and

total RNA was reverse-transcribed with reverse-transcription (RT) primer. PCR products were loaded onto 1.1% agarose gels. Blots were quantified using ImageJ (n=3). The values of each group are indicated relative to the intensity of lane 1. (**E**) MCF10A expressing WT H3 and the T45A mutant were treated with ADR and 0.1mM 5-ethynyl Uridine (EU) for 18 hours. Total RNA was purified and EU-labeled RNA was biotinylated by copper-catalyzed cycloaddition reaction, followed by purification on streptavidine magnetic beads. RNA bound beads were washed and reverse transcribed with RT primers. Synthesized cDNAs were analyzed by real-time qPCR with indicated primers. (**F**) ChIP assay was performed with anti-RNA PolII. Real-time PCR was performed with primers corresponding to TTS of indicated genes. Real-time qPCR and ChIP assay data shown are the average value of at least three independent experiments. Standard deviations are indicated as error bars. * $p<0.05$ ** $p<0.01$ *** $p<0.001$.

4. DISCUSSION

In this study, we demonstrated that AKT-mediated phosphorylation of H3-T45 regulates transcription termination by showing that the inhibition of AKT or the T45A mutation affects the occupancy of RNA PolII downstream of the poly(A) site (Figure 2-5 F). Based on previous reports that downstream RNA 3' of the poly(A) site is degraded by the exonucleolytic Rat1 (XRN2 in humans)/Rai1 complex, which participates in RNA PolII transcription termination, per the torpedo model (39,42), it needs to investigate whether the phosphorylation of H3-T45 is involved in the recruitment of this exonuclease for transcription termination.

DNA damage induces histone phosphorylation to maintain genomic stability. For example, H2AX-Ser139 is phosphorylated primarily at DNA double-strand breaks and recruits damage repair complexes (43,44), and H3-Thr11 is dephosphorylated by chk1 depletion, suppressing transcription of cell cycle-related genes (7). Unlike H3-Thr11 dephosphorylation, which occurs in promoter regions of genes that are repressed on DNA damage, we observed that H3-T45 phosphorylation facilitates the transcriptional activation of DNA damage-inducible genes.

Judging from our data, AKT itself is unlikely to differentiate targets for transcription termination, because a significant amount of H3-T45 phosphorylation simply followed RNA PolII-S2 phosphorylation (Figure 2-3 F and G). Also, H3-T45 phosphorylation was not observed in housekeeping genes, in which RNA PolII-S2 phosphorylation signals were minimal (Figure

2-3 H). It is possible that the factors that correlate with PolII-S2 phosphorylation (CDK12 for example, is a PolII-S2 kinase that harbors conserved AKT phosphorylation motif and predicted to interact with AKT)(45), recruits AKT into chromatin where transcription termination occurs and thereby allowing AKT to phosphorylate H3-T45 and effect termination (Figure 2-6).

We wondered whether H3-T45 phosphorylation in other processes, such as DNA replication and apoptosis, correlates with transcription termination. Previous studies have observed H3-T45 phosphorylation in various events by relevant kinases: PKC-δ under apoptotic conditions (9), Cdc7 during DNA replication (10), and DYRK1A prior to transcriptional activation (40). Except for AKT2, which binds the *CDH1* promoter with Snail1 to repress transcription (46), a link between H3-T45 phosphorylation and transcription has not been reported. Analogous to H3-S10 phosphorylation, which induces transcriptional activation and chromosomal condensation under disparate circumstances (47,48), H3-T45 phosphorylation may function in diverse pathways under various cellular processes. And also, H3-T45 phosphorylation by kinases above may take part in transcription termination.

AKT isoforms are highly homologous but have distinct tissue expression patterns, activation stimuli, and substrate specificity (49). On DNA damage, AKT1 silencing decreases cell survival, whereas AKT2 silencing has a modest effect (16,50). Thus, AKT1 likely mediates the DNA damage

response. Also, we confirmed that AKT1 phosphorylates H3-T45 more effectively than AKT2 (Figure 2-4), supporting our hypothesis that AKT1 facilitates the transcription of stress-response genes through H3-T45 phosphorylation.

Recent studies claim that defective termination at the 3'-end impairs splicing, enhances RNA degradation, and reduces transcriptional initiation at the promoter (51), suggesting that overall transcriptional efficiency is governed by transcription termination.

In this work, we provide an evidence of the connection between post-translational histone modifications and transcription termination—DNA damage-activated AKT phosphorylates H3-T45 of stress-response genes, which must be expressed acutely, facilitating transcription termination for maximum transcriptional efficiency.

Figure 2-6.

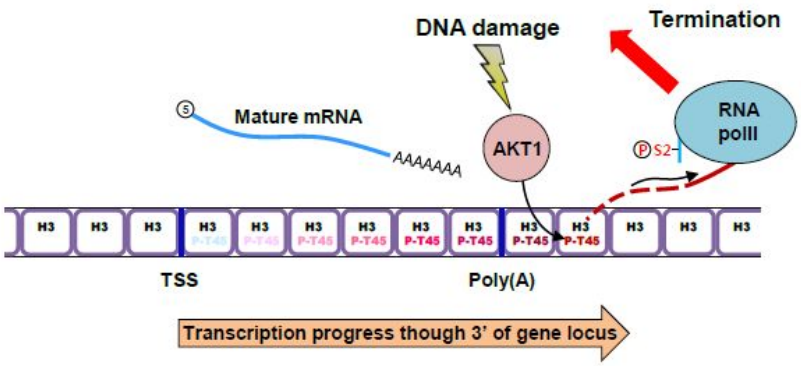

Figure 2-6. Schematic model of AKT1 mediated H3-T45 phosphorylation in transcription termination upon DNA damage.

DNA damage triggers the transcription of stress-response genes by RNA PolII. As transcription progress through 3' of gene locus, RNA PolII-S2 undergoes hyperphosphorylation and DNA damage-activated AKT1 phosphorylates H3-T45. When RNA PolII passes through 3' of poly(A) site, pre-mRNA is cleaved and processes to mature mRNA (26,28). Phosphorylated H3-T45 accelerates the degradation of 5' unprotected RNA downstream of poly(A) site to induce the dissociation of RNA PolII from the chromatin.

5. REFERENCES

1. Campos, E.I. and Reinberg, D. (2009) Histones: annotating chromatin. *Annu. Rev. Genet.*, **43**, 559-599.

2. Jenuwein, T. and Allis, C.D. (2001) Translating the histone code. *Science*, **293**, 1074-1080.

3. Kouzarides, T. (2007) Chromatin modifications and their function. *Cell*, **128**, 693-705.

4. Wei, Y., Yu, L., Bowen, J., Gorovsky, M.A. and Allis, C.D. (1999) Phosphorylation of histone H3 is required for proper chromosome condensation and segregation. *Cell*, **97**, 99-109.

5. Dawson, M.A., Bannister, A.J., Gottgens, B., Foster, S.D., Bartke, T., Green, A.R. and Kouzarides, T. (2009) JAK2 phosphorylates histone H3Y41 and excludes HP1alpha from chromatin. *Nature*, **461**, 819-822.

6. Bunnefeld, N., Borger, L., van Moorter, B., Rolandsen, C.M., Dettki, H., Solberg, E.J. and Ericsson, G. (2011) A model-driven approach to quantify migration patterns: individual, regional and yearly differences. *J. Anim. Ecol.*, **80**, 466-476.

7. Shimada, M., Niida, H., Zineldeen, D.H., Tagami, H., Tanaka, M., Saito, H. and Nakanishi, M. (2008) Chk1 is a histone H3 threonine 11 kinase that regulates DNA damage-induced transcriptional repression. *Cell*, **132**, 221-232.

8. Yang, W., Xia, Y., Hawke, D., Li, X., Liang, J., Xing, D., Aldape, K., Hunter, T., Alfred Yung, W.K. and Lu, Z. (2012) PKM2 phosphorylates histone H3 and promotes gene transcription and tumorigenesis. *Cell*, **150**, 685-696.

9. Hurd, P.J., Bannister, A.J., Halls, K., Dawson, M.A., Vermeulen, M., Olsen, J.V., Ismail, H., Somers, J., Mann, M., Owen-Hughes, T. *et al.* (2009) Phosphorylation of histone H3 Thr-45 is linked to apoptosis. *J. Biol. Chem.*, **284**, 16575-16583.

10. Baker, S.P., Phillips, J., Anderson, S., Qiu, Q., Shabanowitz, J., Smith, M.M., Yates, J.R., 3rd, Hunt, D.F. and Grant, P.A. (2010) Histone H3 Thr 45 phosphorylation is a replication-associated post-translational modification in S. cerevisiae. *Nat. Cell Biol.*, **12**, 294-298.

11. Alessi, D.R., Andjelkovic, M., Caudwell, B., Cron, P., Morrice, N., Cohen, P. and Hemmings, B.A. (1996) Mechanism of activation of protein kinase B by insulin and IGF-1. *EMBO J.*, **15**, 6541-6551.

12. Caporali, S., Levati, L., Starace, G., Ragone, G., Bonmassar, E., Alvino, E. and D'Atri, S. (2008) AKT is activated in an ataxia-telangiectasia and Rad3-related-dependent manner in response to temozolomide and confers protection against drug-induced cell growth inhibition. *Mol. Pharmacol.*, **74**, 173-183.

13. Lu, D., Huang, J. and Basu, A. (2006) Protein kinase Cepsilon activates protein kinase B/Akt via DNA-PK to protect against tumor necrosis factor-alpha-induced cell death. *J. Biol. Chem.*, **281**, 22799-22807.

14. Viniegra, J.G., Martinez, N., Modirassari, P., Hernandez Losa, J., Parada Cobo, C., Sanchez-Arevalo Lobo, V.J., Aceves Luquero, C.I., Alvarez-Vallina, L., Ramon y Cajal, S., Rojas, J.M. *et al.* (2005) Full activation of PKB/Akt in response to insulin or ionizing radiation is mediated through ATM. *J. Biol. Chem.*, **280**, 4029-4036.

15. Brognard, J., Clark, A.S., Ni, Y. and Dennis, P.A. (2001) Akt/protein kinase B is constitutively active in non-small cell lung cancer cells and promotes cellular survival and resistance to chemotherapy and radiation. *Cancer Res.*, **61**, 3986-3997.

16. Bozulic, L., Surucu, B., Hynx, D. and Hemmings, B.A. (2008) PKBalpha/Akt1 acts downstream of DNA-PK in the DNA double-strand break response and promotes survival. *Mol. Cell*, **30**, 203-213.

17. Li, Y., Dowbenko, D. and Lasky, L.A. (2002) AKT/PKB phosphorylation of p21Cip/WAF1 enhances protein stability of p21Cip/WAF1 and promotes cell survival. *J. Biol. Chem.*, **277**, 11352-11361.

18. Mayo, L.D. and Donner, D.B. (2001) A phosphatidylinositol 3-kinase/Akt pathway promotes translocation of Mdm2 from the cytoplasm to the nucleus. *Proc. Natl. Acad. Sci. U. S. A.*, **98**, 11598-11603.

19. Pugazhenthi, S., Nesterova, A., Sable, C., Heidenreich, K.A., Boxer, L.M., Heasley, L.E. and Reusch, J.E. (2000) Akt/protein kinase B up-regulates Bcl-2 expression through cAMP-response element-binding protein. *J. Biol. Chem.*, **275**, 10761-10766.

20. Ozes, O.N., Mayo, L.D., Gustin, J.A., Pfeffer, S.R., Pfeffer, L.M. and Donner, D.B. (1999) NF-kappaB activation by tumour necrosis factor requires the Akt serine-threonine kinase. *Nature*, **401**, 82-85.

21. Brunet, A., Bonni, A., Zigmond, M.J., Lin, M.Z., Juo, P., Hu, L.S., Anderson, M.J., Arden, K.C., Blenis, J. and Greenberg, M.E. (1999) Akt promotes cell survival by phosphorylating and inhibiting a Forkhead transcription factor. *Cell*, **96**, 857-868.

22. Cross, D.A., Alessi, D.R., Cohen, P., Andjelkovich, M. and Hemmings, B.A. (1995) Inhibition of glycogen synthase kinase-3 by insulin mediated by protein kinase B. *Nature*, **378**, 785-789.

23. Maniatis, T. and Reed, R. (2002) An extensive network of coupling among gene expression machines. *Nature*, **416**, 499-506.

24. Corden, J.L. (1990) Tails of RNA polymerase II. *Trends Biochem. Sci.*, **15**, 383-387.

25. Kuehner, J.N., Pearson, E.L. and Moore, C. (2011) Unravelling the means to an end: RNA polymerase II transcription termination. *Nat. Rev. Mol. Cell Biol.*, **12**, 283-294.

26. Rosonina, E., Kaneko, S. and Manley, J.L. (2006) Terminating the transcript: breaking up is hard to do. *Genes Dev.*, **20**, 1050-1056.

27. Logan, J., Falck-Pedersen, E., Darnell, J.E., Jr. and Shenk, T. (1987) A poly(A) addition site and a downstream termination region are required for efficient cessation of transcription by RNA polymerase II in the mouse beta maj-globin gene. *Proc. Natl. Acad. Sci. U. S. A.*, **84**, 8306-8310.

28. Connelly, S. and Manley, J.L. (1988) A functional mRNA polyadenylation signal is required for transcription termination by RNA polymerase II. *Genes Dev.*, **2**, 440-452.

29. Richard, P. and Manley, J.L. (2009) Transcription termination by nuclear RNA polymerases. *Genes Dev.*, **23**, 1247-1269.

30. Jang, H., Choi, S.Y., Cho, E.J. and Youn, H.D. (2009) Cabin1 restrains p53 activity on chromatin. *Nat. Struct. Mol. Biol.*, **16**, 910-915.

31. Langmead, B., Trapnell, C., Pop, M. and Salzberg, S.L. (2009) Ultrafast and memory-efficient alignment of short DNA sequences to the human genome. *Genome Biol.*, **10**, R25.

32. Zhang, Y., Liu, T., Meyer, C.A., Eeckhoute, J., Johnson, D.S., Bernstein, B.E., Nusbaum, C., Myers, R.M., Brown, M., Li, W. *et al.* (2008) Model-based analysis of ChIP-Seq (MACS). *Genome Biol.*, **9**, R137.

33. Heinz, S., Benner, C., Spann, N., Bertolino, E., Lin, Y.C., Laslo, P., Cheng, J.X., Murre, C., Singh, H. and Glass, C.K. (2010) Simple combinations of lineage-determining transcription factors prime cis-regulatory elements required for macrophage and B cell identities. *Mol. Cell*, **38**, 576-589.

34. McLean, C.Y., Bristor, D., Hiller, M., Clarke, S.L., Schaar, B.T., Lowe, C.B., Wenger, A.M. and Bejerano, G. (2010) GREAT improves functional interpretation of cis-regulatory regions. *Nat. Biotechnol.*, **28**, 495-501.

35. Shen, L., Shao, N., Liu, X. and Nestler, E. (2014) ngs.plot: Quick mining and visualization of next-generation sequencing data by integrating genomic databases. *BMC Genomics*, **15**, 284.

36. Kurz, E.U., Douglas, P. and Lees-Miller, S.P. (2004) Doxorubicin activates ATM-dependent phosphorylation of multiple downstream targets in part through the generation of reactive oxygen species. *J. Biol. Chem.*, **279**, 53272-53281.

37. Kau, T.R., Schroeder, F., Ramaswamy, S., Wojciechowski, C.L., Zhao, J.J., Roberts, T.M., Clardy, J., Sellers, W.R. and Silver, P.A. (2003) A chemical genetic screen identifies inhibitors of regulated nuclear export of a Forkhead transcription factor in PTEN-deficient tumor cells. *Cancer Cell*, **4**, 463-476.

38. Endo, H., Nakabayashi, Y., Kawashima, S., Enomoto, T., Seki, M. and Horikoshi, M. (2012) Nucleosome surface containing nucleosomal DNA entry/exit site regulates H3-K36me3 via association with RNA polymerase II and Set2. *Genes Cells*, **17**, 65-81.

39. Kim, M., Krogan, N.J., Vasiljeva, L., Rando, O.J., Nedea, E., Greenblatt, J.F. and Buratowski, S. (2004) The yeast Rat1 exonuclease promotes transcription termination by RNA polymerase II. *Nature*, **432**, 517-522.

40. Jang, S.M., Azebi, S., Soubigou, G. and Muchardt, C. (2014) DYRK1A phoshorylates histone H3 to differentially regulate the binding of HP1 isoforms and antagonize HP1-mediated transcriptional repression. *EMBO Rep*, **15**, 686-694.

41. Brazil, D.P. and Hemmings, B.A. (2001) Ten years of protein kinase B signalling: a hard Akt to follow. *Trends Biochem. Sci.*, **26**, 657-664.

42. Luo, W., Johnson, A.W. and Bentley, D.L. (2006) The role of Rat1 in coupling mRNA 3'-end processing to transcription termination: implications for a unified allosteric-torpedo model. *Genes Dev.*, **20**, 954-965.

43. Rossetto, D., Avvakumov, N. and Cote, J. (2012) Histone phosphorylation: a chromatin modification involved in diverse nuclear events. *Epigenetics*, **7**, 1098-1108.

44. van Attikum, H. and Gasser, S.M. (2005) The histone code at DNA breaks: a guide to repair? *Nat. Rev. Mol. Cell Biol.*, **6**, 757-765.

45. Hornbeck, P.V., Kornhauser, J.M., Tkachev, S., Zhang, B., Skrzypek, E., Murray, B., Latham, V. and Sullivan, M. (2012) PhosphoSitePlus: a comprehensive resource for investigating the structure and function of experimentally determined post-translational modifications in man and mouse. *Nucleic Acids Res.*, **40**, D261-270.

46. Villagrasa, P., Diaz, V.M., Vinas-Castells, R., Peiro, S., Del Valle-Perez, B., Dave, N., Rodriguez-Asiain, A., Casal, J.I., Lizcano, J.M., Dunach, M. *et al.* (2012) Akt2 interacts with Snail1 in the E-cadherin promoter. *Oncogene*, **31**, 4022-4033.

47. Liokatis, S., Stutzer, A., Elsasser, S.J., Theillet, F.X., Klingberg, R., van Rossum, B., Schwarzer, D., Allis, C.D., Fischle, W. and Selenko, P. (2012) Phosphorylation of histone H3 Ser10 establishes a hierarchy for subsequent intramolecular modification events. *Nat. Struct. Mol. Biol.*, **19**, 819-823.

48. Thomson, S., Clayton, A.L. and Mahadevan, L.C. (2001) Independent dynamic regulation of histone phosphorylation and acetylation during immediate-early gene induction. *Mol. Cell*, **8**, 1231-1241.

49. Gonzalez, E. and McGraw, T.E. (2009) The Akt kinases: isoform specificity in metabolism and cancer. *Cell Cycle*, **8**, 2502-2508.

50. Kim, I.A., Bae, S.S., Fernandes, A., Wu, J., Muschel, R.J., McKenna, W.G., Birnbaum, M.J. and Bernhard, E.J. (2005) Selective inhibition of Ras, phosphoinositide 3 kinase, and Akt isoforms increases the radiosensitivity of human carcinoma cell lines. *Cancer Res.*, **65**, 7902-7910.

51. Mapendano, C.K., Lykke-Andersen, S., Kjems, J., Bertrand, E. and Jensen, T.H. (2010) Crosstalk between mRNA 3' end processing and transcription initiation. *Mol. Cell*, **40**, 410-422.

CHAPTER 3

ATP-citrate lyase regulates cellular senescence via AMPK- and p53-dependent pathway

1. INTRODUCTION

ATP-citrate lyase (ACLY) was initially identified as the 'Citrate cleavage enzyme' in 1959, which converts citrate into acetyl-CoA and oxaloacetate (1). In cytosol, ACLY converts mitochondria-derived citrate into acetyl-CoA (2), which is a vital building block for the endogenous biosynthesis of fatty acids and cholesterol. Acetyl-CoA is also required for acetylation reactions that modify proteins, such as histone acetylation (3). Besides ACLY, eukaryotic cells can generate acetyl-CoA by acetyl-CoA synthetase (ACSS) from acetate (4). However, mammalian cells do not prefer acetate as an energy source, rather utilizing glucose as a carbon substrate, unless exceptional circumstances (5). Thus ACLY is a key enzyme regulating cytosolic acetyl-CoA level and de novo lipogenesis in mammals.

Various types of tumors display enhanced endogenous fatty acid biosynthesis, which fuels membrane biogenesis in rapidly proliferating cancer cells (5). ACLY is upregulated or activated in several types of cancers, including lung, prostate, bladder, breast, liver, stomach, and colon tumors (6-10). The elevation of ACLY activity and expression status in cancer cells suggests that ACLY inhibition may be an attractive approach for cancer therapy (5). Inhibition of ACLY by either RNAi or pharmacologic inhibitors results in growth arrest in tumor cells, both *in vitro* and *in vivo* (2, 6). The anti-proliferative effects of ACLY suppression are mediated by cell-cycle arrest (2, 6) and induction of apoptosis (11). The molecular mechanism underlying ACLY-silencing-induced proliferation arrest is not clear yet. One

possibility is that ACLY-silencing-induced proliferation arrest is due to fatty acid starvation. However, fatty acid supplementation does not rescue cancer cells from the proliferation arrest mediated by ACLY-knockdown (6), suggesting an additional function of ACLY in tumorigenesis.

Senescent cells undergo distinct morphological alterations, showing typical enlarged and flattened shape. Senescent cells are discriminated from normal cells with the expression of biomarkers of senescence, including positive staining for β-galactosidase and increased p53, p21, p16, p27 expression (5). It is well-known that tumor suppressor protein p53 plays a central role in cellular senescence (12-14). AMP-activated protein kinase (AMPK) is a cellular sensor, responding to metabolic stresses to maintain energy homeostasis (15). It is known that cell cycle arresting under energy deficient conditions is triggered by p53, which is activated by AMPK (16). AMPK, activated by metabolic stress, induces the phosphorylation of p53 on serine 15 and prolonged activation of AMPK leads to p53-dependent cellular senescence (16).

In this study we found that ACLY-silencing induces cellular senescence in normal cells. ACLY physically interacted with AMPK and inhibited AMPK activity. Furthermore ACLY-silencing activated p53 pathway and facilitated DNA-damage-induced apoptosis in both normal and cancer cells. These findings suggest that metabolic enzyme ACLY regulates cellular senescence through protein-protein interaction as well as its enzymatic activity.

2. MATERIALS AND METHODS

1. Lentiviral sh-RNA-mediated knockdown of ACLY

Lentiviral vectors containing the human ACLY-targeting sequences pLKO.1-sh-ACLY #1 (TRCN0000291890), #2 (TRCN0000291815), #3 (TRCN0000291817), #4 (TRCN0000222698), and #5 (TRCN0000078283) were purchased from Sigma. As a control, the pLKO.1 vector was used. Lentivirus was produced according to the manufacturer's protocol using the BLOCK-iT Lentiviral RNAi expression system (Invitrogen). Twenty-four hours after lentiviral infection, infected cells were selected with puromycin (1 μg/ml) for 2 weeks and then used for experiments. Because pLKO.1-sh-ACLY #3 was most effective, we used it in most experiments, where it is not specifically noted.

2. Cell culture and transient expression

Primary Human Dermal Fibroblasts (HDF) cells, HEK293T and HCT116 cells were described previously (17). HDF cells were cultured in Dulbecco's modified Eagle's medium supplemented with 10% (v/v) fetal bovine serum and antibiotics and then transfected using Lipofectamine (Invitrogen), according to the manufacturer's instructions. Polyethylenimine (PEI, polysciences, Inc.) was used to transfect HEK293T cells.

3. DNA constructs

Mammalian expression vector for p53 are described previously (17, 18). Expression vectors for ATP citrate lyase and AMPK were obtained by inserting PCR fragments into pcDNA3.1-Myc and pcDNA3-HA (Invitrogen).

4. Antibodies

Anti-Actin, anti-Flag (M2) antibodies were purchased from Sigma; anti-HA (16B12) and anti-Myc (9E10) from Covance; anti-p53 (DO-1) and anti-p21 from Santa Cruz Biotechnology; anti-H3 and anti-H3 (acetylated) from Abcam; anti-AMPKα and anti-phospho-AMPKα (Thr172) from Cell Signaling; anti-ACLY was generated by Abfrontier (Seoul, Korea) with immunizing peptide, corresponding amino acid sequence to ACLY into SPF rabbits.

5. Animals

Harlan Sprague-Dawley (SD) rats were described previously (19). Rats were purchased and maintained from the Animal Laboratory of Seoul National University College of Medicine. Old animals were maintained on a normal diet for more than 30 month. 6-month-old female rats were used as young controls. All animals were handled in accordance with the guidelines of the Korea Food and Drug Administration.

6. Immunohistochemistry

Paraffin tissue sections were deparaffinized with xylene and graded ethanol, and antigen retrieval was performed by heating the sections in 10mM sodium citrate buffer (pH 6.0) at 95° C for 30 min. After washing, sections were blocked with 2% hydrogen peroxide in methanol at 4°C for 30 min. The slides were then washed again with DW and incubated with horse serum for 1 hour to suppress nonspecific binding. Samples were incubated with 1:50 anti-ACLY antibody in PBS at 4°C overnight. Visualization was performed using 3,3'-DAB (Sigma). All immunostained sections were counterstained with Mayer's hematoxylin.

7. Immunofluorescent staining

Immunofluorescent staining was carried out as described previously (20). Briefly, cells on the cover glasses were fixed with 4% (w/v) paraformaldehyde, permeabilized with 0.5% (v/v) Triton X-100, and blocked with 2% (w/v) bovine serum albumin in phosphate-buffered saline. Endogenous ACLY and acetyl-H3 were immunostained with corresponding rabbit antibody and Rhodamine Red-X conjugated secondary anti-rabbit antibody with anti-p53 mouse antibody and FITC-conjugated secondary anti-mouse IgG antibody (Jackson Immunoresearch). 50% (v/v) glycerol containing 4′,6-diamidino-2-phenylindole solutions are loaded on the slide glass and covered with cover glass. Immunofluorescence was observed under a Zeiss LSM 510 laser scanning microscope.

8. Real-time PCR analysis of relative mRNA levels.

Real-time qPCR analysis was carried out as described previously (21). Briefly, Total RNA was extracted with TriZol (Invitrogen) and reverse-transcribed (AMV Reverse Transcriptase XL, Life science, Co). mRNA levels were quantified by real-time PCR with the SYBR Green qPCR Kit (Finnzymes, F-410L) on the iQ5 and CFX connect Real-time PCR Detection System (Bio-Rad) and then normalized to actin. All data shown are the average of at least three independent experiments and standard deviations are indicated as error bars. Sequences of the primers used for mRNA quantification were described in Table 1-1.

9. Senescence-associated β-gal staining

Cells growing on the culture plates were washed twice with PBS, fixed with 4% paraformaldehyde, washed with PBS. Cells were incubated in 37°C with X-gal solution [1mg/ml X-gal (USB corporation, Cleveland, OH USA), 40mM Sodium citrate-pH 6.0 (Sigma), 5mM Potassium ferrocyanide (Sigma), 5mM Potassium ferricyanide (Sigma), 150mM NaCl, 2mM $MgCl_2$] and observed under Nikon ECLIPSE TS100 phase-contrast microscope.

10. Flow cytometry analysis

Flow cytometry analysis was carried out as described previously (18). Briefly, cells were harvested and washed three times with PBS. Cells were then incubated with FITC Annexin-V (BD Pharmingen) and propidium iodide (Sigma) for 15 min and analyzed by flow cytometry (Beckman Coulter). At least 10,000 cells were collected and analyzed with the Coulter Epics XL™

flow cytometer (Beckman-Coulter, USA). Percentages of cells were calculated with Multicycle for Windows software (Beckman-Coulter).

11. Immunoprecipitation and Western Blot

Cells were lysed with lysis buffer [20 mM Tris-HCl (pH 7.4), 150 mM NaCl, 0.5% (v/v) NP-40, 1×protease inhibitor cocktail (Roche)], and cell lysates were incubated with the appropriate antibody in the presence of protein A/G beads (Santa Cruz Biotechnology). Immunoprecipitates were boiled with SDS sample buffer, loaded into SDS-PAGE gels, transferred to nitrocellulose membranes and probed with suitable antibodies.

12. *In vitro* AMPK kinase assay

Anti-Myc conjugated protein G agarose bead was used to immunoprecipitate HEK293T cells overexpressing pcDNA3-HA-AMPKα2 in total cell lysates. Immunoprecipitated protein G agarose bead was mixed with GST or GST-SAMS in 15 mM HEPES, 6.25 mM β-glycerol phosphate, 1.25 mM EGTA, 0.45 mM dithiothreitol, 18.75 mM $MgCl_2$, 125 μM ATP, 150 μM AMP, 10 μCi ^{32}P-ATP (IZOTOP, Hungary) with or without His-ACLY. Reaction mixture was incubated 0.5 hours at 30℃ and loaded onto SDS-PAGE. Gels were dried 1 hour at 80℃ and exposed on X-ray film for overnight at -80℃.

13. Purification of recombinant proteins

Proteins of GST-AMPKα2 and His_6-ACLY were generated by subcloning PCR fragment into pGEX4T-1 (Amersham Biosciences) or pRSETB (Invitrogen). GST-SAMS was generated by inserting synthesized oligonucleotides corresponding to SAMS peptide into pGEX4T-1. GST fusion proteins were expressed in the Escherichia-coli strain *DH5α* and proteins were isolated using Glutathione Sepharose™ 4B beads (Amersham Biosciences), according to the manufacturer's instructions. His_6 fusion proteins were expressed in the strain *BL21DE3* and proteins were purified with Ni-NTA agarose (Quiagen), according to the manufacturer's instructions.

ACTB (Actin)	Forward	5′-GGCATCCACGAAACTACCTT-3′
	Reverse	5′-CTGTGTGGACTTGGGAGAGG-3′
CDKN1A (p21)	Forward	5′-GCAGACCAGCATGACAGATTT-3′
	Reverse	5′-GGATTAGGGCTTCCTCTTGGA-3′
ACLY	Forward	5′-GGGCTTACGGGTGATGGGAG-3′
	Reverse	5′-GAAGTTTGCAGTGTGGGCCG-3′
Gadd45	Forward	5′-TGCTCAGCAAAGCCCTGAGT-3′
	Reverse	5′-GCTTGGCCGCTTCGTACA-3′
Bax	Forward	5′-GAGGATGATTGCTGACGTGGAC-3′
	Reverse	5′-GCCATGTGGGGGTCCCGAAG-3′
Puma	Forward	5′-ACTGTGAATCCTGTGCTCTGCC-3′
	Reverse	5′-CAAATGAATGCCAGTGGTCACAC-3′

Table 3-1. Primers used in Chapter 3

3. RESULTS

1. ACLY-knockdown triggers cellular senescence in normal cells

ACLY inhibition result in retarded proliferation of cancer cells, probably blocking *de-novo* lipogenesis by acetyl-CoA production, which is required for cellular membrane biosynthesis (5-10) for rapidly proliferating cancer cells. However, fatty acid supplementation could not recover the retarded growth of cancer cells by ACLY inhibition (6). Hence, we hypothesized that ACLY could have additional function beyond acetyl-CoA production.

To understand the role of ACLY, we silenced ACLY using lentivirus containing shRNAs against ACLY in primary human cells, which proliferates relatively slower than cancer cells. Efficient knockdown of ACLY in primary HDF cells was confirmed by Western Blot (Figure 3-1 A). Interestingly, ACLY-knockdown cells showed apparent growth retardation and a typical senescent morphology (flat and enlarged in size). Proliferation assay and senescence-associated β-gal (SA-β-gal) staining showed that knockdown of ACLY in HDF cells significantly reduced its proliferation rate (Figure 3-1 B). A large portion of ACLY-knockdown cells were positive for SA-β-gal staining (Figure 3-1 C, D).

To test the correlation of ACLY with cellular senescence, we compared the protein level of ACLY between young (8 passages) and old (32 passages) HDF cells. The protein level of ACLY was significantly reduced in old HDF cells compared to its younger counterparts (Figure 3-1. E).

We investigated that this phenomenon was reproducible in different types of rat tissues. Tissues from 6 and 30 month old rats (19) were analyzed by immunohistochemistry and Western Blot. ACLY protein was substantially down-regulated in brain, liver, and kidney of older rats by immunohistochemistry (Figure 3-1 F). Western Blot also showed that ACLY protein level was reduced in brain, liver, and adipose tissue of older rats (Figure 3-1 G). These findings suggest that downregulation of ACLY correlates with cellular senescence in normal cells.

Figure 3-1.

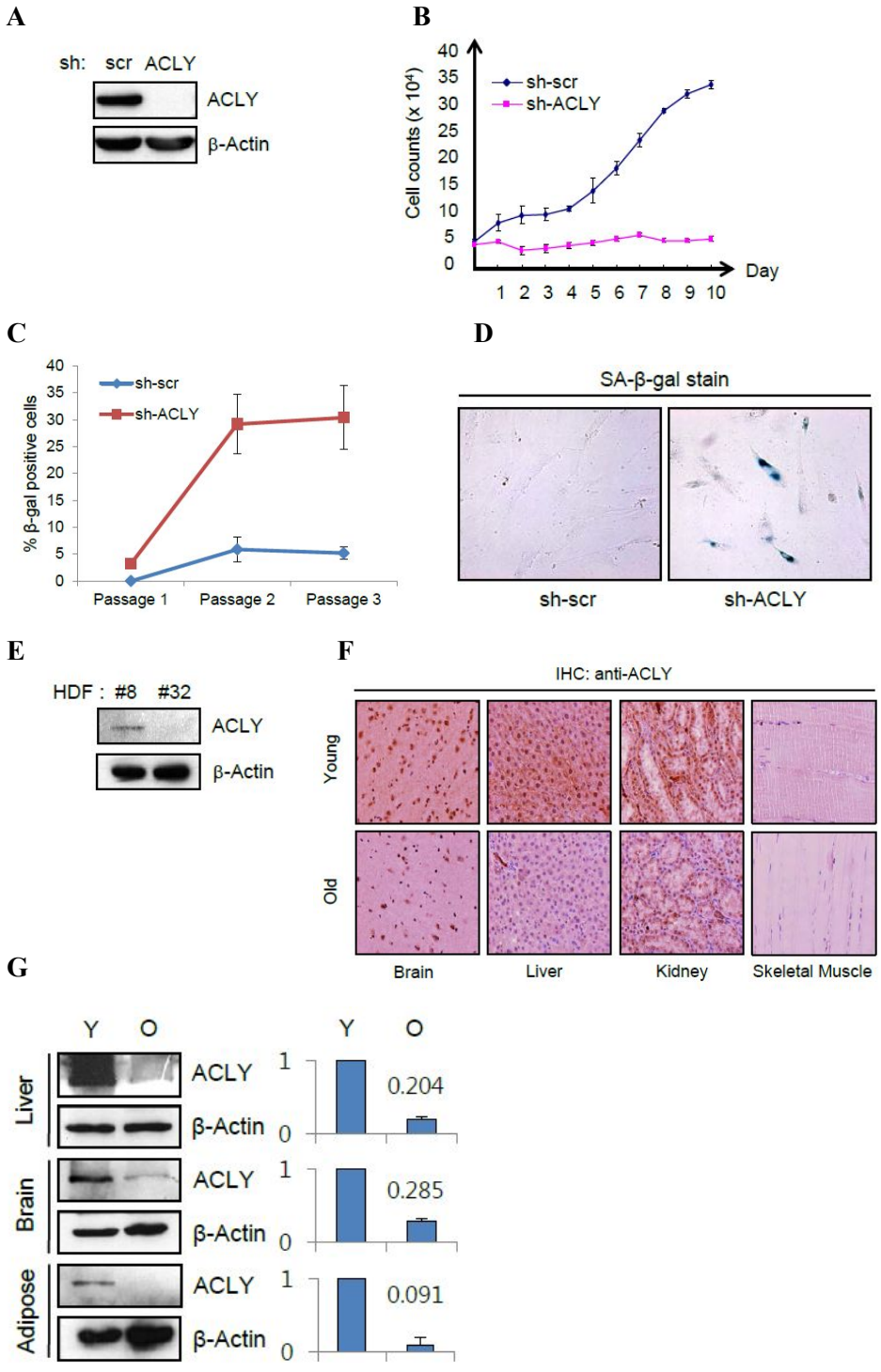
A
sh: scr ACLY
ACLY
β-Actin
B
Cell counts (x 10⁴)
sh-scr
sh-ACLY
Day
C
% β-gal positive cells
sh-scr
sh-ACLY
Passage 1
Passage 2
Passage 3
D
SA-β-gal stain
sh-scr
sh-ACLY
E
HDF : #8 #32
ACLY
β-Actin
F
IHC: anti-ACLY
Young
Old
Brain
Liver
Kidney
Skeletal Muscle
G
Y O
Y O
Liver
Brain
Adipose
ACLY
β-Actin
0.204
0.285
0.091

Figure 3-1. ACLY-knockdown triggers cellular senescence in normal cells. (**A**) Whole cell lysates from scrambled and sh-ACLY lentivirus infected HDF were probed for Western Blot with anti-ACLY antibody. (**B**) Scrambled or ACLY-knockdown HDF cells were cultured in normal growth media and proliferation of cells were analyzed. (**C**), Scrambled or ACLY-knockdown HDF cells were stained for SA-β-gal after infection of sh-RNA. Passage 1; 3 days post infection, Passage 2; 10 days, Passage 3; 17days, respectively. (**D**) Representative image of cells on passage 2 of (C). (**E**) Whole cell lysates from different passages of HDF cells were probed for Western Blot using anti-ACLY antibody. (**F**) Immunohistochemistry of 6 and 30 months old Sprague Dawley (SD) rat tissues. (**G**) Total cell extracts from tissues of rat used in (F) were probed for Western Blot using anti-ACLY antibody. Blot quantification was performed by Image J software (normalized to β-Actin, relative value to the blot of young samples, n=2).

2. ACLY-silencing-induced cellular senescence is dependent on p53 pathway

The tumor suppressor protein p53 has been shown to play critical roles in the induction of senescence (22). Thus we tested whether ACLY-silencing is related to p53-induced cellular senescence. Initially, we silenced p53 in ACLY-knockdown HDF cells, and found that additional knockdown of p53 completely abrogated ACLY-silencing-induced cellular senescence (Figure 3-2 A-B).

We tested whether p53 protein was affected by ACLY-silencing. As a result, we could observe elevated p53 protein level in ACLY-knockdown HDF cells by confocal microscopy (Figure 3-2 C).

Consistent with elevated p53 protein level, we could also observe increased mRNA levels of p53 downstream target genes (18), such as p21, Gadd45, bax, and noxa, which are closely related to cell cycle and apoptosis regulation, by real-time qPCR (Figure 3-2 D).

Figure 3-2.

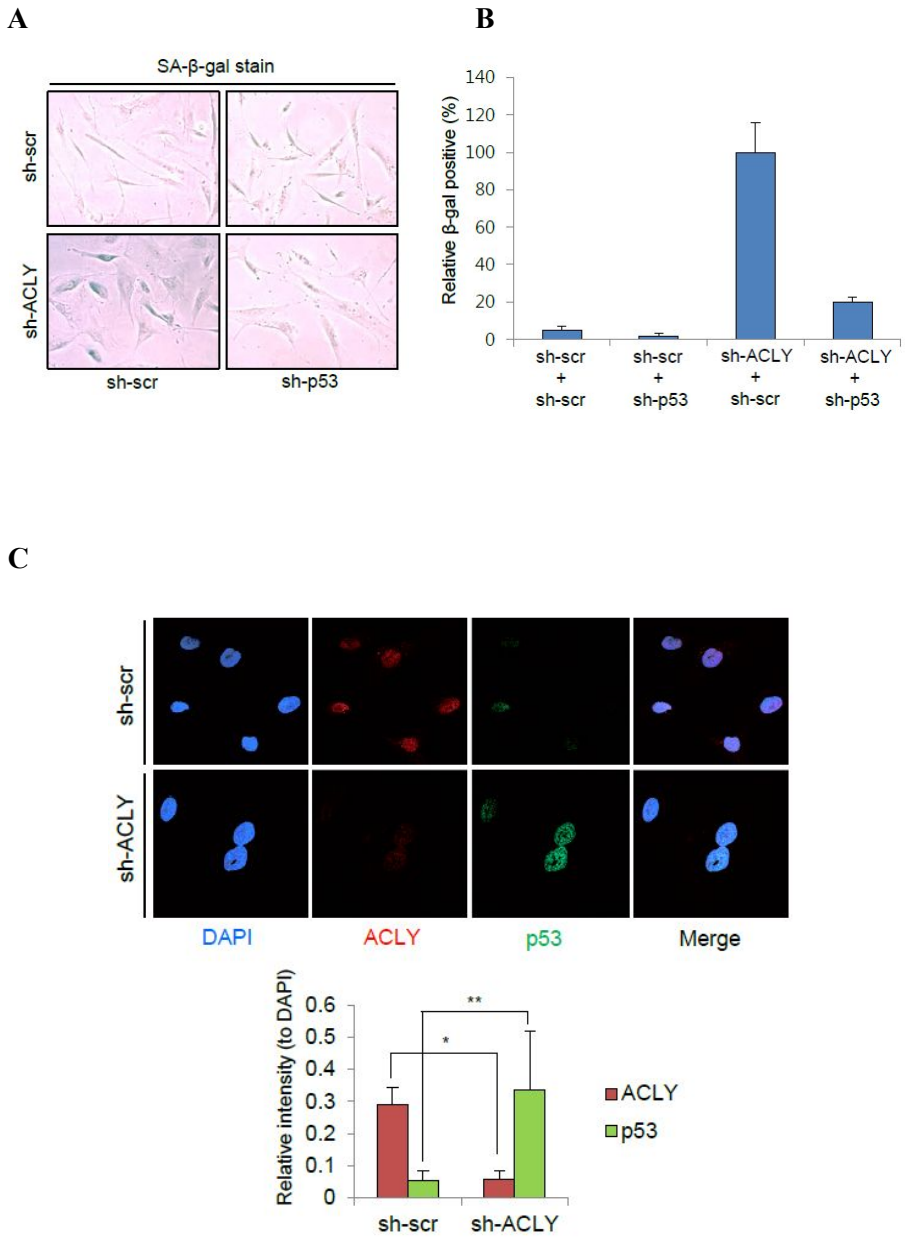
A
SA-β-gal stain
sh-scr
sh-ACLY
sh-scr
sh-p53
B
Relative β-gal positive (%)
140
120
100
80
60
40
20
0
sh-scr + sh-scr
sh-scr + sh-p53
sh-ACLY + sh-scr
sh-ACLY + sh-p53
C
sh-scr
sh-ACLY
DAPI
ACLY
p53
Merge
Relative intensity (to DAPI)
0.6
0.5
0.4
0.3
0.2
0.1
0
**
*
ACLY
p53
sh-scr
sh-ACLY

Figure 3-2.

D

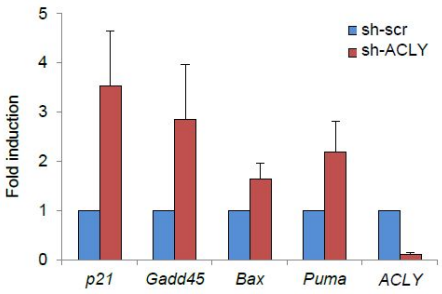

Figure 3-2. ACLY-silencing-induced cellular senescence is dependent on p53 pathway.

(**A**) Scrambled or ACLY-knockdown HDF cells were additionally knocked down for scrambled or p53 and stained for senescence associated-β-gal. (**B**) Calculated SA-β-gal positive portion of HDF cells in (A). (**C**) Scrambled or ACLY-knockdown HDF cells were fixed and stained for confocal microscopy with anti-ACLY (red) and anti-p53 (green). The signal intensities of individual cells are indicated (normalized to DAPI). **p*=0.0012, ***p*=0.017 (**D**) Real-time qPCR analysis using cDNA, reverse-transcribed from the RNA of Scrambled or ACLY-knockdown HDF cells.

3. ACLY-silencing-induced senescence is independent on acetyl-CoA level

Because ACLY is a key enzyme regulating cytosolic acetyl-CoA level and acetyl-CoA is critical for various biochemical processes, we postulated that ACLY-silencing-induced p53 activation and cellular senescence may be dependent on acetyl-CoA level. Recently, ACLY was reported to regulate histone acetylation by acetyl-CoA processing (3), thus histone acetylation status can represent cellular acetyl-CoA level.

In primary HDF cells, knockdown of ACLY significantly reduced the level of histone H3 acetylation (Figure 3-3 A, +PBS). Since acetyl-CoA is impermeable to cells, external addition of acetyl-CoA cannot restore cellular acetyl-CoA level. Acetyl-CoA synthetase (ACSS) runs an alternative acetyl-CoA production pathway (4). Thus we postulated that addition of acetate in culture medium could rescue the reduced cellular acetyl-CoA level caused by ACLY-silencing. Indeed, addition of acetate restored histone H3 acetylation level in ACLY-knockdown HDF cells (Figure 3-3 A, +NaOAc).

Next, we tested whether the senescent phenotype is a consequence of the altered status of acetyl-CoA level caused by ACLY-knockdown. SA-β-gal staining showed that the addition of acetate in culture medium did not alleviate ACLY-silencing-induced cellular senescence (Figure 3-3 B) nor decreased the elevated p21 mRNA level, caused by ACLY-knockdown

(Figure 2-3 C). These findings suggest that ACLY-silencing-induced p53 activation and cellular senescence is independent of cellular acetyl-CoA level.

Figure 3-3.

A

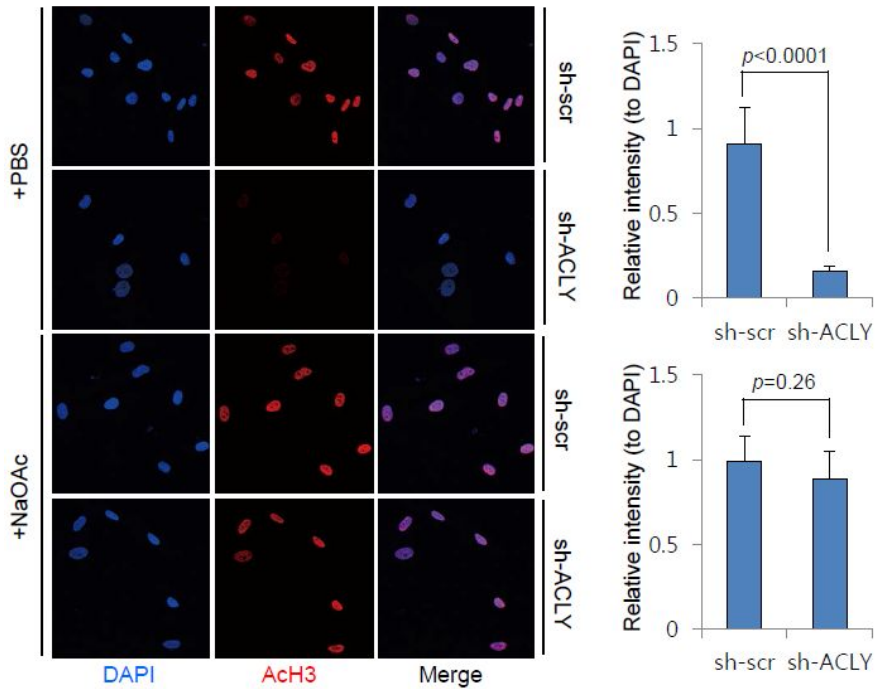
+PBS
+NaOAc
sh-scr
sh-ACLY
sh-scr
sh-ACLY
DAPI
AcH3
Merge
Relative intensity (to DAPI)
p<0.0001
1.5
1
0.5
0
sh-scr
sh-ACLY
Relative intensity (to DAPI)
p=0.26
1.5
1
0.5
0
sh-scr
sh-ACLY

B

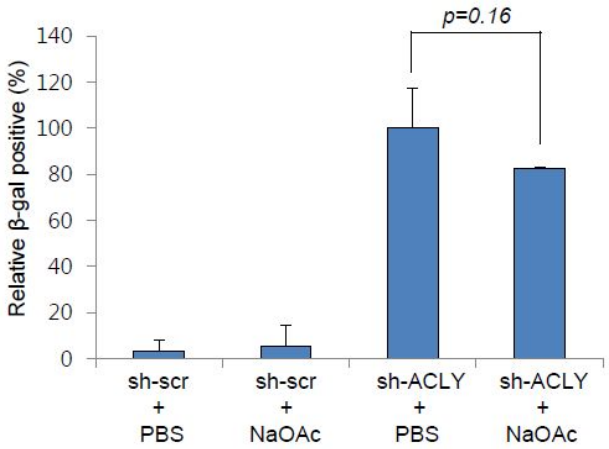
p=0.16
Relative β-gal positive (%)
140
120
100
80
60
40
20
0
sh-scr + PBS
sh-scr + NaOAc
sh-ACLY + PBS
sh-ACLY + NaOAc

Figure 3-3.

C

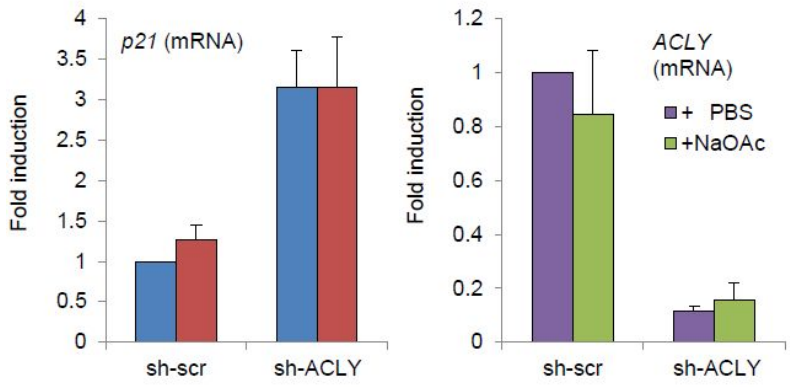

Figure 3-3. ACLY-silencing-induced senescence is independent on acetyl-CoA level.

Scrambled or ACLY-knockdown HDF cells were treated with PBS or 5mM sodium acetate (NaOAc), (**A**) fixed and stained for confocal microscopy with anti-acetylated histone H3. The signal intensities of individual cells are indicated (normalized to DAPI). (**B**) SA-β-gal positive cells were calculated (relative percent value compared to the sh-ACLY+PBS set to 100%, average value of three independent experiments counting 200 cells per experiment), (**C**) p21 or ACLY mRNA was quantified by realtime-qPCR analysis.

4. ACLY physically interacts with AMPK and inhibits AMPK activity

Because ACLY activated p53 in a cellular acetyl-CoA-independent manner, we speculated that ACLY regulates p53 by physical interaction. Co-immunoprecipitation assay showed that there was no physical interaction between ACLY and p53 (Figure 3-4 A).

Since prolonged activation of AMPK leads to p53 dependent cellular senescence (16), we tested whether ACLY-silencing activates AMPK. Western Blot showed substantial increase of phosphorylated-AMPK not only in ACLY-knockdown HDF cells, but also in old HDF cells and rat adipose tissue (Figure 3-4 B, C).

To examine the physical interaction between ACLY and AMPK, we performed a co-immunoprecipitation assay. In mammals, AMPK exists in heterotrimeric form which consists of one catalytic subunit termed α and two regulatory subunits termed β and γ (23). We could observe the interaction of ACLY with AMPK $\alpha 2$ subunit and not with β and γ subunit (Figure 3-4 D, E). The direct interaction of ACLY with AMPK $\alpha 2$ was confirmed by *in vitro* GST-pulldown assay (Figure 3-4 F).

By immunofluorescent staining of overexpressed AMPK and endogenous ACLY, we could observe over 25% and 37% of the signal co-localized in HDF and HCT116 cells, respectively (Figure 3-4 G). And *in vitro* kinase

assay using immunoprecipitated AMPK α2 showed apparent reduction of AMPK activity by ACLY (Figure 3-4 H).

These findings suggest that ACLY physically inhibits catalytic subunit of AMPK, and ACLY-knockdown might have triggered the AMPK-mediated activation of p53.

Figure 3-4.

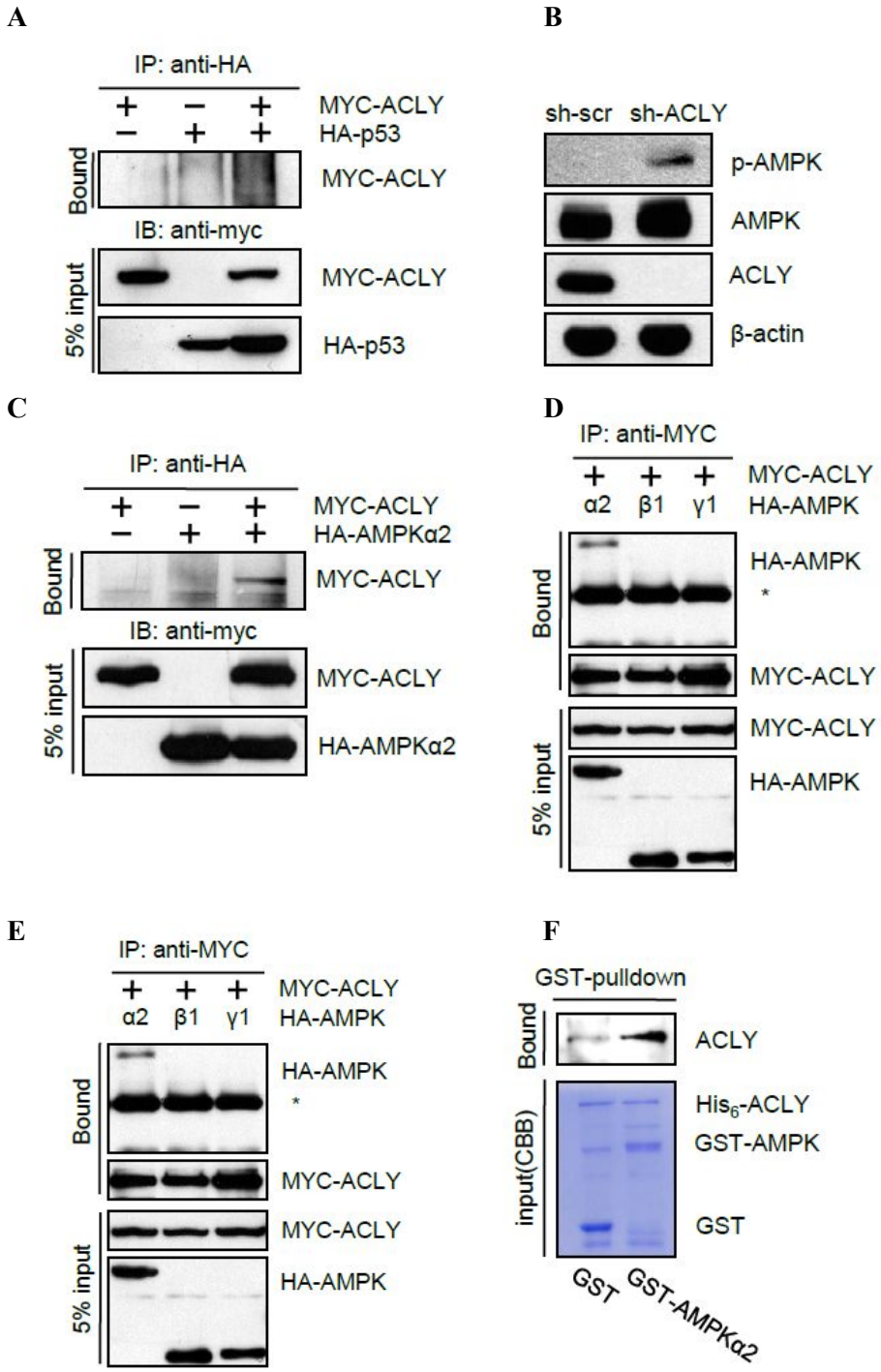
A
IP: anti-HA
MYC-ACLY
HA-p53
Bound
MYC-ACLY
IB: anti-myc
5% input
MYC-ACLY
HA-p53
B
sh-scr
sh-ACLY
p-AMPK
AMPK
ACLY
β-actin
C
IP: anti-HA
MYC-ACLY
HA-AMPKα2
Bound
MYC-ACLY
IB: anti-myc
5% input
MYC-ACLY
HA-AMPKα2
D
IP: anti-MYC
MYC-ACLY
α2 β1 γ1
HA-AMPK
Bound
HA-AMPK
*
MYC-ACLY
5% input
MYC-ACLY
HA-AMPK
E
IP: anti-MYC
MYC-ACLY
α2 β1 γ1
HA-AMPK
Bound
HA-AMPK
*
MYC-ACLY
5% input
MYC-ACLY
HA-AMPK
F
GST-pulldown
Bound
ACLY
input(CBB)
His6-ACLY
GST-AMPK
GST
GST
GST-AMPKα2

Figure 3-4.

G

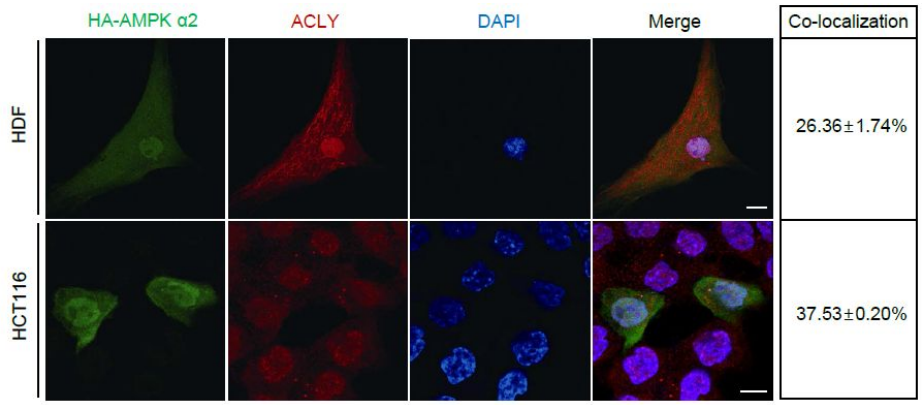

H

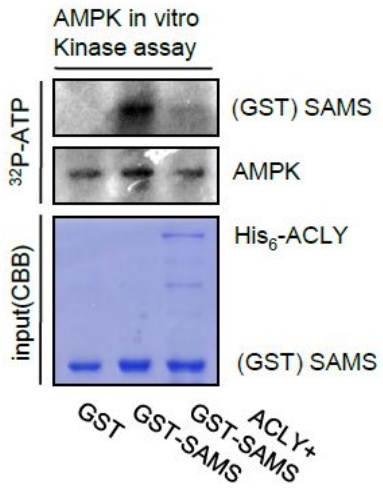

Figure 3-4. ACLY physically interacts with AMPK and inhibits AMPK activity. (**A**) MYC-ACLY and HA-tagged p53 were co-transfected into HEK293T cells. After 48-hr post transfection, cells were collected, lysed and immunoprecipitated with anti-HA antibody. Immunoprecipitates were probed

with anti-MYC antibody. (**B**) Whole cell lysates of scrambled and ACLY-knockdown HDF cells were probed for Western Blot with indicated antibodies. (**C**) Whole cell lysates of young (passage 8)/old (passage 32) HDF cells and young (6 months)/old (30 months) rat adipose tissues were probed for Western blot. (**D**) MYC-ACLY and HA-AMPK α2 were co-transfected into HEK293T cells. Whole cell lysates were immunoprecipitated with anti-HA antibody and probed with anti-MYC antibody. (**E**) MYC-ACLY and HA-tagged α2, β1, γ1 subunits of AMPK were co-transfected into HEK293T cells, immunoprecipitated with anti-MYC antibody and probed for Western Blot using anti-HA antibody. (**F**) GST-AMPKα2 and His_6-ACLY purified from bacteria, were precipitated with Glutathione Sepharose 4B beads, washed and eluted. Elutes were probed for Western Blot with anti-ACLY antibody. (**G**) HA-AMPKα2, overexpressed HDF and HCT116 cells were stained with anti-HA (green) and anti-ACLY (red) antibody. Colocalization of two signals were quantified by Leica application suite software, means ± s.d. ($n \geq 3$) are shown. DNA counterstained with DAPI. Scale bar, 10 μm. (**H**) HA-AMPKα2, overexpressed in HEK293T cells were immunoprecipitated with protein G agarose bead. *In vitro* AMPK kinase assay was performed with GST or GST-SAMS as a substrate with/without His_6-ACLY.

5. ACLY-knockdown facilitates DNA-damage-induced apoptosis in both normal and cancer cells

Since we found that ACLY regulates proliferation via p53 in normal cells, we questioned whether similar molecular mechanism may exist in cancer cells. ACLY was knocked down in HCT116 human colon cancer cells, which express wild type p53 (18), and p53 activation status was analyzed by Western Blot. Knockdown of ACLY not only increased p53 protein level, but also p53 activation marker (phosphorylated serine 15) (Figure 3-5 A), indicating that ACLY-silencing induces p53 activation in cancer cells.

Activation of p53 facilitates DNA-damage-induced apoptosis in cancer cells (18). Thus we tested whether knockdown of ACLY also facilitates DNA-damage-induced apoptosis. ACLY-knockdown HCT116 cells were exposed to UV irradiation and stained with Annexin V and propidium iodide, then analyzed with flow-cytometry. Upon UV irradiation, ACLY-knockdown increased early-apoptotic cells more than 10% compared to control (Figure 3-5 B). Normal HDF cells also showed similar phenomena (Figure 3-5 C).

On the basis of these results, we propose a molecular mechanism by which ACLY-silencing leads to cellular senescence and tumor suppression (Figure 3-5 D). During aging process, the declined level of ACLY protein causes chronic activation of AMPK, which can lead to p53-activated cellular senescence. This process might contribute to anti-tumor development. Moreover, in tumors harboring high level of ACLY (2, 6-10), ACLY-

knockdown could sensitize cells to DNA-damaging anti-tumor drugs via p53 pathway.

Figure 3-5.

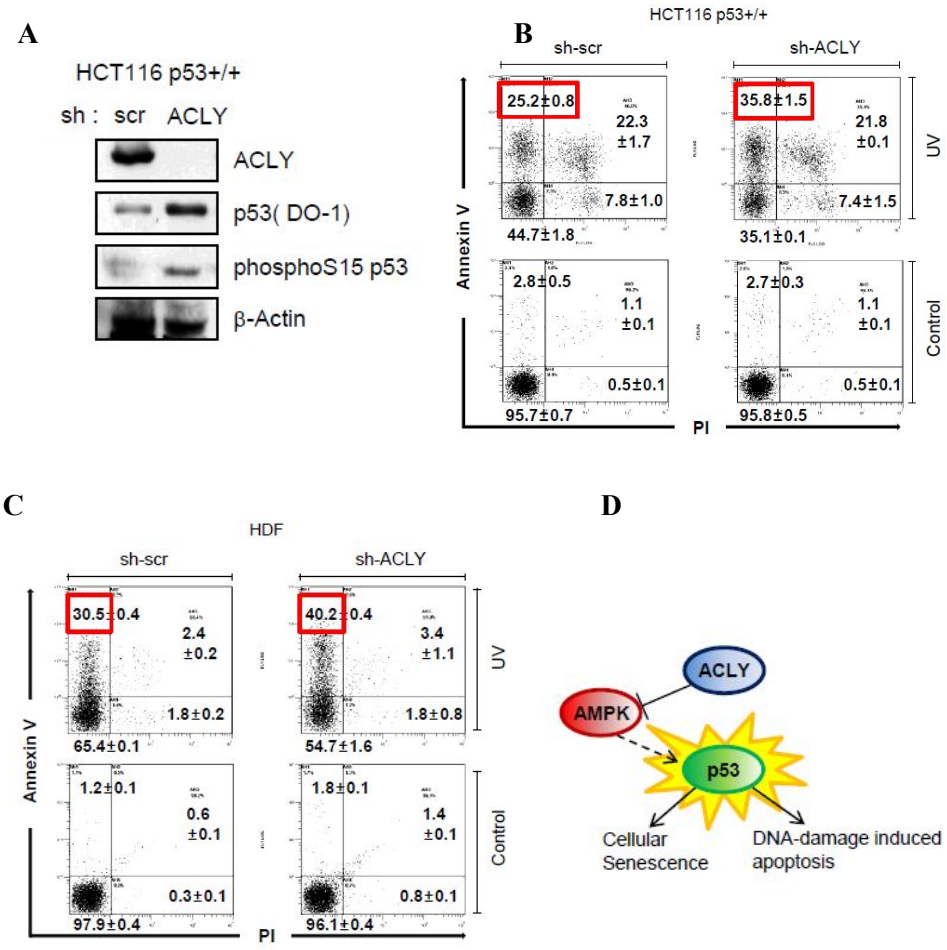

Figure 3-5. ACLY-knockdown facilitates DNA-damage-induced apoptosis in both normal and cancer cells.

(**A**) Whole cell lysates from scrambled and ACLY-knockdown in HCT116 cells were probed for Western Blot with indicated antibodies. (**B**), (**C**) Scrambled and ACLY-knockdown HCT116 and HDF cells were treated with/without 100J/m^2 UV irradiation. 48 hours later (72 hours for HDF cells), cells were fixed, double-stained with propidium iodide and Annexin V-FITC,

and analyzed with flow cytometry. A representative figure and means ± s.d. (n=2) are shown (**D**) Schematic model of ACLY-silencing-induced tumor suppression. ACLY down-regulation activates AMPK and activated AMPK may facilitate p53-induced cellular senescence or apoptosis which leads to tumor suppression.

4. DISCUSSION

In this study we showed that ACLY declines during aging in human and rat cells (Figure 3-1), which is consistent with previous reports studied in rodents (24-26). In yeast, acetyltransferase NuA4 acetylates Sip2, a regulatory β subunit of the Snf1 complex (yeast AMPK), inhibiting its catalytic activity (27). Although this phenomenon is not evaluated on mammalian cells, it suggests that AMPK is activated during aging process.

The activity of p53 has been known to be enhanced during aging process (12-14). Our study suggests that ACLY-knockdown may cause AMPK activation and then p53 activation during aging process. Moreover, we showed that ACLY-knockdown cells displayed decreased proliferation rate and senescent phenotype (Figure 3-1). Thus ACLY-knockdown might trigger cellular senescence by activating AMPK-p53.

The activities of central metabolic enzymes are regulated by acetylation (28). Thus, insufficient acetyl-CoA caused by ACLY-knockdown might have caused metabolic stress, leading to cellular senescence. However, supplying additional acetate into culture media cannot alleviate ACLY-knockdown induced senescence, although it sufficiently recovers the reduced acetylation level of histone H3 in ACLY-knockdown cells (Figure 3-3) This finding suggests that ACLY has additional function beyond its original role in producing acetyl-CoA.

In cells undergoing metabolic stress, AMPK is phosphorylated and activated, induces p53 stabilization (16). Although we could not detect any direct physical interaction between ACLY and p53 protein, we found substantial increase of phosphorylated-AMPK in ACLY-knockdown cells. And increased phosphorylated-AMPK might stabilize p53, which leads to cellular senescence. Previous study also agrees with our data that baseline levels of phosphorylated-AMPK were higher in aged brains compared to young mice (29). In addition, ACLY directly interacted with AMPK protein, in particular, catalytic α subunit, and suppressed its kinase activity (Figure 3-4).

Our study revealed that ACLY-knockdown triggers p53 activation, which causes increased apoptosis of cancer cells. ACLY-knockdown stabilized p53 in human colon cancer cells, which results in enhanced apoptotic activity under DNA damaging condition (Figure 3-5). Moreover, emerging evidences claim cellular senescence as an 'evasive maneuver' against tumorigenesis (30-32). Despite the nature of decreasing ACLY by aging process still needs to be uncovered, we propose a novel function of ACLY in cellular senescence and tumorigenesis.

5. REFERENCES

1. Srere PA (1959) The citrate cleavage enzyme. I. Distribution and purification. *J Biol Chem* **234**, 2544-7.

2. Hatzivassiliou G, Zhao F, Bauer DE, Andreadis C, Shaw AN, Dhanak D, Hingorani SR, Tuveson DA & Thompson CB (2005) ATP citrate lyase inhibition can suppress tumor cell growth. *Cancer Cell* **8(4)**, 311-21.

3. Wellen KE, Hatzivassiliou G, Sachdeva UM, Bui TV, Cross JR & Thompson CB (2009) ATP-citrate lyase links cellular metabolism to histone acetylation. *Science* **324(5930),** 1076-80.

4. Yoshii Y, Furukawa T, Yoshii H, Mori T, Kiyono Y, Waki A, Kobayashi M, Tsujikawa T, Kudo T, Okazawa H, Yonekura Y & Fujibayashi Y (2009) Cytosolic acetyl-CoA synthetase affected tumor cell survival under hypoxia: the possible function in tumor acetyl-CoA/acetate metabolism. *Cancer Sci* **100(5)**, 821-7.

5. Zaidi N, Swinnen JV & Smans K (2012) ATP-citrate lyase: a key player in cancer metabolism. *Cancer Res* **72(15)**, 3709-14.

6. Migita T, Narita T, Nomura K, Miyagi E, Inazuka F, Matsuura M, Ushijima M, Mashima T, Seimiya H, Satoh Y, Okumura S, Nakagawa K, & Ishikawa Y (2008) ATP citrate lyase: activation and therapeutic implications in non-small cell lung cancer. *Cancer Res* **68(20)**, 8547-54.

7. Yancy HF, Mason JA, Peters S, Thompson CE 3rd, Littleton GK, Jett M & Day AA (2007) Metastatic progression and gene expression between breast cancer cell lines from African American and Caucasian women. *J Carcinog* **6**, 8.

8. Varis A, Wolf M, Monni O, Vakkari ML, Kokkola A, Moskaluk C, Frierson H Jr, Powell SM, Knuutila S, Kallioniemi A & El-Rifai W (2002) Targets of gene amplification and overexpression at 17q in gastric cancer. *Cancer Res* **62(9)**, 2625-9.

9. Turyn J, Schlichtholz B, Dettlaff-Pokora A, Presler M, Goyke E, Matuszewski M, Kmieć Z, Krajka K & Swierczynski J (2003) Increased activity of glycerol 3-phosphate dehydrogenase and other lipogenic enzymes in human bladder cancer. *Horm Metab Res* **35(10)**, 565-9.

10. Halliday KR, Fenoglio-Preiser C & Sillerud LO (1988) Differentiation of human tumors from nonmalignant tissue by natural-abundance 13C NMR spectroscopy. *Magn Reson Med* **7(4)**, 384-411.

11. Hanai J, Doro N, Sasaki AT, Kobayashi S, Cantley LC, Seth P & Sukhatme VP (2012) Inhibition of lung cancer growth: ATP citrate lyase knockdown and statin treatment leads to dual blockade of mitogen-activated protein kinase (MAPK) and phosphatidylinositol-3-kinase (PI3K)/AKT pathways. *J Cell Physiol* **227(4)**, 1709-20.

12. Kuilman T, Michaloglou C, Mooi WJ & Peeper DS (2010) The essence of senescence. *Genes Dev* **24(22)**, 2463-79.

13. Rufini A, Tucci P, Celardo I & Melino G (2013) Senescence and aging: the critical roles of p53. *Oncogene* **32(43)**, 5129-43.

14. Itahana K, Dimri G & Campisi J (2001) Regulation of cellular senescence by p53. *Eur J Biochem* **268(10)**, 2784-91.

15. Hardie DG, Carling D & Carlson M (1998) The AMP-activated/SNF1 protein kinase subfamily: metabolic sensors of the eukaryotic cell? *Annu Rev Biochem* **67**, 821-55.

16. Jones RG, Plas DR, Kubek S, Buzzai M, Mu J, Xu Y, Birnbaum MJ & Thompson CB (2005) AMP-activated protein kinase induces a p53-dependent metabolic checkpoint. *Mol Cell* **18(3)**, 283-93.

17. Lee SM, Kim JH, Cho EJ & Youn HD (2009) A nucleocytoplasmic malate dehydrogenase regulates p53 transcriptional activity in response to metabolic stress. *Cell Death Differ* **16(5)**, 738-48.

18. Jang H, Choi SY, Cho EJ & Youn HD (2009) Cabin1 restrains p53 activity on chromatin. *Nat Struct Mol Biol* **16(9)**, 910-5.

19. Choi JW, Kim JH, Cho SC, Ha MK, Song KY, Youn HD & Park SC (2011) Malondialdehyde inhibits an AMPK-mediated nuclear translocation

and repression activity of ALDH2 in transcription. *Biochem Biophys Res Commun* **404(1)**, 400-6.

20. Lee JH, Jang H, Cho EJ & Youn HD (2009) Ferritin binds and activates p53 under oxidative stress. *Biochem Biophys Res Commun* **389(3)**, 399-404.

21. Jang H, Kim TW, Yoon S, Choi SY, Kang TW, Kim SY, Kwon YW, Cho EJ & Youn HD (2012) O-GlcNAc regulates pluripotency and reprogramming by directly acting on core components of the pluripotency network. *Cell Stem Cell* **11(1)**, 62-74.

22. Ben-Porath I & Weinberg RA (2005) The signals and pathways activating cellular senescence. *Int J Biochem Cell Biol* **37(5)**, 961-76.

23. Neumann D, Woods A, Carling D, Wallimann T & Schlattner U (2003) Mammalian AMP-activated protein kinase: functional, heterotrimeric complexes by co-expression of subunits in Escherichia coli. *Protein Expr Purif* **30(2)**, 230-7.

24. Hoffmann GE, Kreisel C, Wieland OH & Weiss L (1979) Pyruvate dehydrogenase and ATP citrate (pro-3S)-lyase activities in adipose tissue and liver of the young lean and the older obese rat. *Hoppe Seylers Z Physiol Chem* **360(1)**, 45-50.

25. Nogalska A, Pankiewicz Z, Goyke E & Swierczynski J (2003) The age-related inverse relationship between ob and lipogenic enzymes genes expression in rat white adipose tissue. *Exp Gerontol* **38(4)**, 415-22.

26. Beigneux AP, Kosinski C, Gavino B, Horton JD, Skarnes WC & Young SG (2004) ATP-citrate lyase deficiency in the mouse. *J Biol Chem* **279(10)**, 9557-64.

27. Lu JY , Lin YY, Sheu JC , Wu JT , Lee FJ , Chen Y , Lin MI , Chiang FT , Tai TY , Berger SL , Zhao Y , Tsai KS , Zhu H , Chuang LM & Boeke JD (2011) Acetylation of yeast AMPK controls intrinsic aging independently of caloric restriction. *Cell* **146(6)**, 969-79.

28. Wang Q, Zhang Y, Yang C, Xiong H, Lin Y, Yao J, Li H, Xie L, Zhao W, Yao Y, Ning ZB, Zeng R, Xiong Y, Guan KL, Zhao S & Zhao GP (2010) Acetylation of metabolic enzymes coordinates carbon source utilization and metabolic flux. *Science* **327(5968)**, 1004-7.

29. Liu F1, Benashski SE, Persky R, Xu Y, Li J & McCullough LD (2012) Age-related changes in AMP-activated protein kinase after stroke. *Age (Dordr)* **34(1)**, 157-68.

30. Campisi J & d'Adda di Fagagna F (2007) Cellular senescence: when bad things happen to good cells. *Nat Rev Mol Cell Biol* **8**, 729–40.

31. Prieur A & Peeper DS (2008) Cellular senescence *in vivo*: a barrier to tumorigenesis. *Curr Opin Cell Biol* **20**, 150–55.

32. Collado M & Serrano M (2010) Senescence in tumours: evidence from mice and humans. *Nat Rev Cancer* **10**, 51–57.

CHAPTER 4

Conclusion

In these studies, we have found that H3-T45 is phosphorylated by DNA damage-activated AKT. By genome-wide ChIP-sequencing analysis, we found that phosphorylated H3-T45 resides predominantly at the TTS of DNA damage response genes. This specific TTS occupancy of phosphorylated H3-T45 closely resembled the transcription termination marker phosphorylated RNA-PolII S2. AKT1 was more effective in H3-T45 phosphorylation than AKT2 isoform. T45 phosphorylation defective mutant H3 expressing cells showed abnormal 3' end processing of DNA damage response genes, and resulted in retarded RNA-PolII dissociation from the chromatin.

ACLY silencing showed reduced proliferation and cellular senescence in HDF cells. Various tissues from old rat showed reduced expression of ACLY protein compared to their younger counterparts. The cellular senescence was p53 dependent, and the protein level of p53 was increased in ACLY knockdown HDF cells. There were no physical interaction between ACLY and p53 protein. However, ACLY knockdown cells as well as old rat tissue showed increased phosphorylated AMPK. ACLY directly interacted with AMPKα2 subunit and inhibited its catalytic activity.

In summary, we have found that H3-T45 phosphorylation marks transcription termination on DNA damage response genes to facilitate overall transcription efficiency. And we also found that decreasing expression of ACLY with ageing chronically activates AMPK, resulting in p53 activation and cellular senescence.

ABSTRACT IN KOREAN

국문 초록

Post-translational modification 은 단백질의 성격을 변화시켜 본래의 기능과는 또 다른 역할을 수행하게 도와준다.

DNA 와 결합하여 chromatin 을 구성하는 히스톤 단백질의 N-terminal tail 부분 수식화는 전체적인 히스톤 단백질의 정전기적 성질을 변화시켜, 전사인자 단백질의 DNA 에 대한 물리적 결합을 조절하거나 N-terminal tail 자체가 전사인자를 동반한 단백질 복합체와 결합하는 부위로 역할을 함으로써 전사활성 조절에서 매우 중요한 역할을 수행한다고 알려져 있다.

p53 은 'guardian of genome' 이라 불릴 만큼 종양생성 과정에서 유전체의 보존에 매우 중요한 단백질로 알려져 있으며 다양한 수식화를 통하여 cell-cycle arrest, DNA-repair, apoptosis 등을 조절하는 것으로 알려져 있다.

본 연구에서는 첫째, DNA 손상 시에 인산화가 이루어지는 새로운 히스톤 수식화에 대한 연구를 수행하였다. 히스톤 H3 의 45 번째 threonine(H3-T45)이 다양한 DNA 손상 조건에서 인산화가 이루어짐을 확인하였으며, 이는 세포 내 신호전달 단백질로 알려져 있는 AKT 에 의해 이루어지는 것을 확인하였다. AKT 는 주로 호르몬이나 성장인자의 자극을 전달하는 serine/threonine kinase 로 세포성장을 유도하여 cellular oncogenesis 에서 역할을

한다고 알려져 있으며, 특히 DNA 손상 조건에서 인산화가 일어나 활성화되어 CDKN1A 의 전사활성을 유도하여 세포 생존에 중요한 역할을 한다고 알려져 있다. Genomewide ChIP-sequencing 을 통한 분석 결과 H3-T45 의 인산화는 전사종결을 일으키는 RNA 중합효소 II CTD 의 Ser2 인산화와 매우 유사한 형태로, 주로 활발하게 진행되는 유전자의 전사 종결부위에서 높게 나타남을 확인하였다. AKT1 단백질이 AKT2 단백질 보다 H3-T45 의 인산화에 미치는 영향이 큰 것으로 나타났으며, 아미노산 치환을 통해 H3-T45 의 인산화를 억제한 경우에 mRNA 절단부위 하위에서 RNA 의 분해가 저해됨을 확인하였고 RNA 중합효소와 염색질의 분리도 저해됨을 확인하였다. 본 실험을 통해 DNA 손상 시에 인산화가 유도되는 새로운 히스톤 수식화인 H3-T45 의 인산화가 유전자 전사에 중요한 역할을 수행하고 있다는 새로운 사실을 발견하였다.

둘째, p53 을 통한 cellular senescence 를 조절하는 단백질로써 ATP citrate lyase 에 대한 연구를 수행하였다. ATP citrate lyase (ACLY)는 세포 내의 citrate 를 이용해 acetyl-CoA 를 생성하여 지방합성에 관여하는 단백질로 알려져 있으며, 이러한 특성 때문에 암세포에서 ACLY 를 저해시키면 암세포의 성장을 억제하는 것으로 알려져 있다. 최근의 연구결과 ACLY 는 acetyl-CoA 합성을 통해 histone acetylation 을 조절하여 전반적인 유전자 발현에 영향을 미치는 것으로 밝혀졌다. 본 실험에서는 정상세포 내 ACLY 의

억제가 cellular senescence 를 유발하는 현상을 발견하였고, 이것이 p53 을 통해 일어난다는 사실을 확인하였다. 또한, ACLY 가 저해된 세포에 acetyl-CoA 를 넣어주었을 경우에도 senescent phenotype 으로부터 회복하지 못했으며 ACLY 가 AMPK 단백질과 직접 결합함으로써 AMPK 의 활성을 억제하고 있음을 확인하였다. 정상세포에서의 경우와 마찬가지로, 암세포에서 ACLY 의 억제는 p53 의 활성화를 야기함으로써 DNA 손상조건에서 세포사멸을 증가시켰다. 본 실험을 통하여 cellular senescence 와 tumorigenesis 에서 세포 내 에너지 sensor 인 AMPK 와 종양억제자 단백질인 p53 을 연결 짓는 ACLY 의 새로운 기능을 발견하였다.

주요어 : **ATP-citrate lyase (ACLY), p53, AMP-activated protein kinase (AMPK), senescence, tumor, AKT, histone, phosphorylation, DNA-damage, transcription, transcription termination**

학 번 : 2009-30609